USGS
science for a changing world

Prepared in cooperation with the Bureau of Land Management

Estimates of Groundwater Discharge by Evapotranspiration, Stump Spring and Hiko Springs, Clark County, Southern Nevada, 2016–18

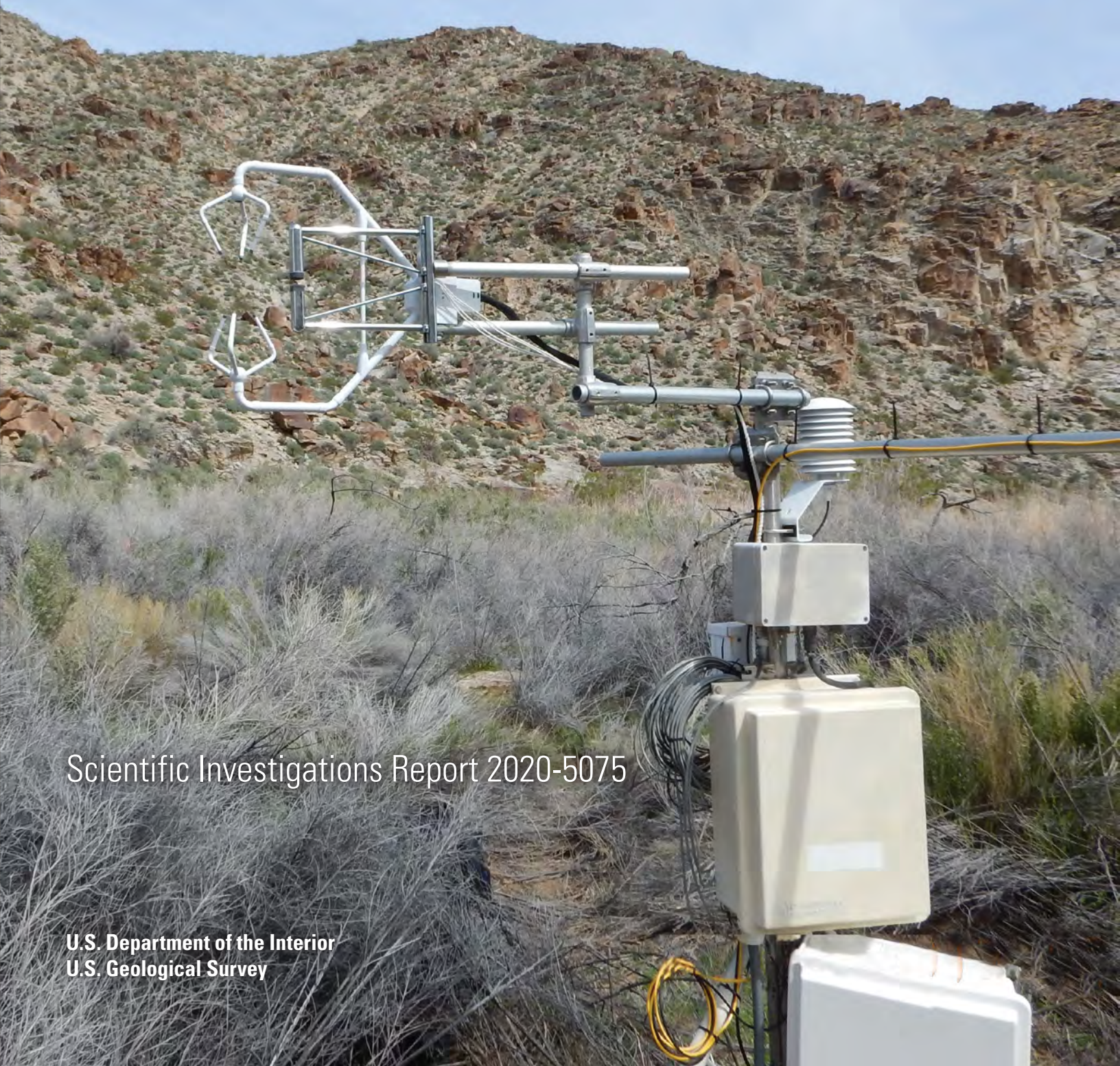

Scientific Investigations Report 2020-5075

U.S. Department of the Interior
U.S. Geological Survey

Cover: Eddy covariance evapotranspiration station at Hiko Spring, Clark County, southern Nevada. Photograph by Michael T. Moreo, U.S. Geological Survey, March 8, 2017.

Estimates of Groundwater Discharge by Evapotranspiration, Stump Spring and Hiko Springs, Clark County, Southern Nevada, 2016–18

By Michael T. Moreo, Susan G. Buto, David W. Smith, and Nora C. Nelson

Prepared in cooperation with the Bureau of Land Management

Scientific Investigations Report 2020–5075

U.S. Department of the Interior
U.S. Geological Survey

U.S. Department of the Interior
DAVID BERNHARDT, Secretary

U.S. Geological Survey
James F. Reilly II, Director

U.S. Geological Survey, Reston, Virginia: 2020

Suggested citation:
Moreo, M.T., Buto, S.G., Smith, D.W., and Nelson, N.C., 2020, Estimates of groundwater discharge by evapotranspiration, Stump Spring and Hiko Springs, Clark County, southern Nevada, 2016–18: U.S. Geological Survey Scientific Investigations Report 2020–5075, 39 p., https://doi.org/10.3133/sir20205075.

Associated data for this publication:
Buto, S.G., 2020, Geospatial data to support estimates of annual groundwater discharge by evapotranspiration from areas of spring-fed riparian vegetation, Stump Spring and Hiko Springs, Clark County, southern Nevada: U.S. Geological Survey data release, https://doi.org/10.5066/P9BG3VKP.

Smith, D.W., Moreo, M.T., Buto, S.G., and Nelson, N.C., 2020, Supplemental evapotranspiration gap-filled datasets from Stump Spring and Hiko Springs, Clark County, southern Nevada, 2016–18: U.S. Geological Survey data release, https://doi.org/10.5066/P9KD11GX.

ISSN 2328-0328 (online)

Contents

Figures

Tables

Conversion Factors

U.S. customary units to International System of Units

Multiply	By	To obtain
	Area	
acre	4,047	square meter (m^2)
acre	0.4047	hectare (ha)
	Flow rate	
cubic foot per second (ft^3/s)	0.02832	cubic meter per second (m^3/s)
acre-foot per year (acre-ft/yr)	1,233	cubic meter per year (m^3/yr)
acre-foot per year (acre-ft/yr)	0.001233	cubic hectometer per year (hm^3/yr)

International System of Units to U.S. customary units

Multiply	By	To obtain
	Length	
millimeter (mm)	0.03937	inch (in.)
centimeter (cm)	0.3937	inch (in.)
meter (m)	3.281	foot (ft)
kilometer (km)	0.6214	mile (mi)
	Area	
square meter (m^2)	0.0002471	acre
hectare (ha)	2.471	acre
	Volume	
milliliter (mL)	0.033814	ounce, fluid (fl. Oz)
cubic meter (m^3)	0.0002642	million gallons (Mgal)
cubic meter (m^3)	0.0008107	acre-foot (acre-ft)

Multiply	By	To obtain
	Flow rate	
millimeter per day (mm/d)	0.00328084	foot per day (ft/d)
millimeter per year (mm/yr)	0.03937	inch per year (in/yr)
cubic meter per second (m^3/s)	35.31	cubic foot per second (ft^3/s)
	Mass	
milligram (mg)	0.00003527	ounce, avoirdupois (oz)
gram (g)	0.03527	ounce, avoirdupois (oz)
kilogram (kg)	2.205	pound, avoirdupois (lb)
	Density	
gram per cubic meter (g/m^3)	0.00006242	pound per cubic foot (lb/ft^3)
	Energy	
watt per square meter (W/m^2)	0.0222	calorie per second per square foot ($cal/s/ft^2$)
joule (J)	0.2390	calorie (cal)

Temperature in degrees Celsius (°C) may be converted to degrees Fahrenheit (°F) as follows:

$°F=(1.8×°C)+32$

Datums

Vertical coordinate information is referenced to North American Vertical Datum of 1988 (NAVD 88).

Horizontal coordinate information is referenced to World Geodetic System of 1984 (WGS 84).

Elevation, as used in this report, refers to distance above the vertical datum.

Abbreviations

ACEC	Area of Critical Environmental Concern
AET	actual evapotranspiration
BLM	Bureau of Land Management
CNF	cumulative normalized flux
EBR	energy-balance ratio
G	soil-heat flux
GDA	groundwater discharge area
GWA	groundwater discharge area
GWET	groundwater discharge by evapotranspiration
H	sensible-heat flux
LE	latent-heat flux
NAIP	National Agriculture Imagery Program
NVDI	Normalized Difference Vegetation Index
P	precipitation
PEST	Parameter ESTimation
r^2	coefficient of determination
R_n	net radiation
RMS error	root-mean-squared error
USGS	U.S. Geological Survey
WV-2	WorldView-2
VI	vegetation index

This page intentionally left blank

Estimates of Groundwater Discharge by Evapotranspiration, Stump Spring and Hiko Springs, Clark County, Southern Nevada, 2016–18

By Michael T. Moreo, Susan G. Buto, David W. Smith, and Nora C. Nelson

Abstract

This report documents methodology and results of a study that estimated groundwater discharge by evapotranspiration (*GWET*) from phreatophytic vegetation in two desert riparian areas with ephemeral spring discharge in Clark County, southern Nevada. The phreatophytes consisted primarily of western honey mesquite [*Prosopis glandulosa* var. *torreyana* (L.D. Benson) M.C. Johnst.] at Stump Spring and mixed shrubs at Hiko Springs. An eddy-covariance station and precipitation gage were established to concurrently measure actual evapotranspiration (AET) and precipitation. Site-scale *GWET* rates—computed by subtracting measured precipitation from AET—were 239 ±45 millimeters per year (mm/yr) based on measurements over one growing season at Stump Spring and 109 ±27 mm/yr averaged over two growing seasons at Hiko Springs.

The volume of *GWET* for each groundwater discharge area (GDA) was estimated by developing relations between site-scale computed *GWET* rates and phreatophytic vegetation represented by a Normalized Difference Vegetation Index (NDVI). A GDA was delineated for the natural drainage in each area by mapping the extent of phreatophytes using high-resolution imagery. A second GDA was delineated at Stump Spring by mapping the extent of phreatophytes in the Area of Critical Environmental Concern (ACEC). Site-scale *GWET* rates were scaled up by applying the site-based *GWET* -NDVI relations to NDVI distributions in each GDA. The areas of phreatophytic vegetation within each GDA, area-weighted mean *GWET* rates, and *GWET* volumes were as follows: (1) Stump Spring—59 hectares (ha), 126 mm/yr, $7.4 \pm 1.4 \times 10^4$ cubic meters per year (m^3/yr) (60 ± 11 acre-feet/yr); Stump Spring ACEC—49 ha, 98 mm/yr, $4.9 \pm 0.9 \times 10^4$ m^3/yr (39 ± 7 acre-feet/yr); and (2) Hiko Springs—7.2 ha, 112 mm/yr, $0.8 \pm 0.2 \times 10^4$ m^3/yr (6.6 ±1.6 acre-feet/yr). The *GWET* rate computed at Stump Spring compared favorably with published *GWET* rates for mesquite.

Introduction

Riparian areas account for less than (<) 2 percent of the total land area in the arid southwestern United States (Ffolliott and others, 2004). Their soil and vegetation characteristics are strongly influenced by the presence of water. Water-rich riparian areas have highly diverse habitats that promote greater biodiversity compared to adjacent uplands. Many such riparian areas were altered throughout the 19th and 20th centuries as the American West was settled. As the population of southern Nevada continues to increase, resource managers increasingly are concerned about the future impacts to limited water resources in these environmentally sensitive ecosystems. For many areas of southern Nevada, however, information is limited on consumptive water use by riparian vegetation at groundwater- or spring-dependent ecosystems.

Stump Spring and Hiko Springs are desert riparian areas in southern Nevada characterized by ephemeral springs in lowland washes (fig. 1). Stump Spring has been designated an Area of Critical Environmental Concern (ACEC) by the Bureau of Land Management (BLM). Areas of Critical Environmental Concern are so designated because special management attention is required to protect and prevent irreparable damage to important historic, cultural, or scenic values, fish and wildlife resources, or other natural resources (U.S. Department of Interior, 2001). The riparian vegetation at Stump Spring and Hiko Springs consists primarily of phreatophytes. Phreatophytes can exist in these arid environments because groundwater is shallow and accessible to plant roots, establishing the biological “backbone” of these ecosystems. Accurate estimates of the consumptive use of groundwater by phreatophytes at Stump Spring and Hiko Springs are critical to establish a baseline from which to quantify any future changes to these desert riparian ecosystems that may be caused by groundwater pumping, climate change, or both.

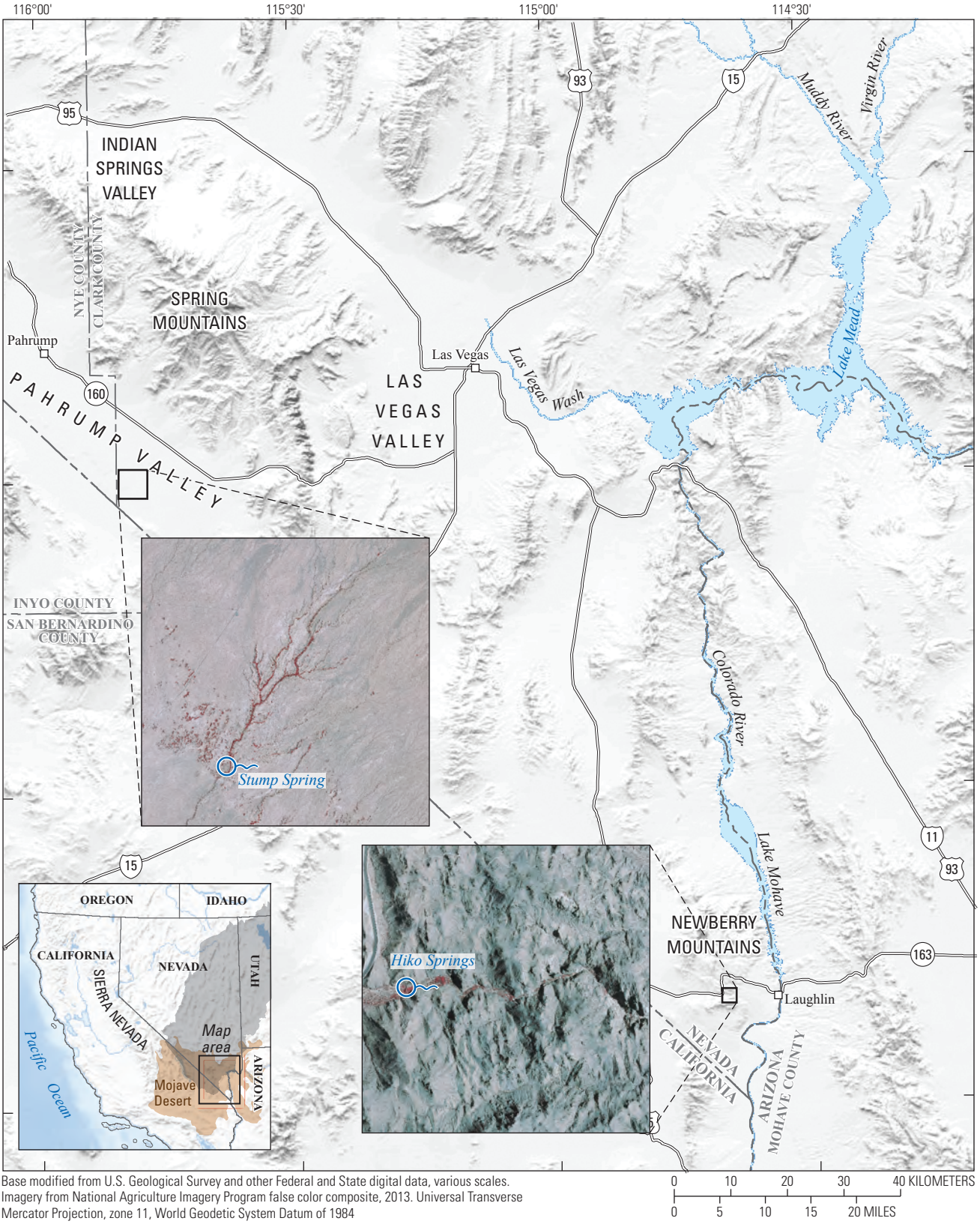

Figure 1. Locations of Stump Spring and Hiko Springs study areas, Clark County, southern Nevada.

In cooperation with the BLM, the U.S. Geological Survey (USGS) conducted a study to estimate groundwater discharge by evapotranspiration (*GWET*) from the phreatophytic vegetation at Stump Spring and Hiko Springs. In Nevada, the amount of groundwater available for appropriation is determined based on the perennial yield, and the perennial yield of a groundwater reservoir ultimately is limited to the maximum amount of natural groundwater discharge that can be salvaged for beneficial use (Nevada Office of the State Engineer, 2007). Groundwater discharge by evapotranspiration (also commonly called groundwater discharge or groundwater evapotranspiration) is defined in this report as the consumptive use of groundwater by phreatophytes. Estimates were derived by distributing site-scale *GWET* rates to each groundwater discharge area (GDA) using aerial imagery and remote-sensing techniques. This methodology has been well-established and consistently applied by the USGS in Nevada over the last 20 years, from about 2000 to 2020. Earlier studies measured actual evapotranspiration (AET) using the Bowen-ratio method (Laczniak and others, 1999, 2001, 2006; Reiner and others, 2002; DeMeo and others, 2003), whereas more recent studies have measured AET using the eddy-covariance method (Moreo and others, 2007, 2017; Laczniak and others, 2008; Garcia and others, 2015; Berger and others, 2016).

Purpose and Scope

This report documents methodology and results of a groundwater discharge investigation at Stump Spring and Hiko Springs. The study objective was to estimate *GWET* from the phreatophytic vegetation in delineated GDAs. An eddy-covariance station and precipitation gage were established in each area to measure AET and precipitation rates. The periods of operation were March 25, 2016–March 6, 2017, at Stump Spring and March 8, 2017–December 7, 2018, at Hiko Springs. Groundwater discharge areas were delineated by identifying and mapping the extent of phreatophytic vegetation based on aerial imagery and remote-sensing techniques. Annual *GWET* estimates and associated uncertainties are reported. Maps showing GDA extents are presented. The *GWET* rate computed for mesquite at Stump Spring was compared to *GWET* rates for mesquite from other areas of the southwestern United States.

This report and the accompanying data releases (Buto, 2020; Smith and others, 2020) are expected to provide baseline estimates of *GWET* that can be used by management agencies to support resource planning. The data generated from this research effort also can be used to support future biophysical and water-availability impact studies—including ecophysiological, climate change, and groundwater recharge and discharge modeling efforts. Moreover, annual *GWET* rate estimates presented in this report can be used to estimate *GWET* in other areas where the hydrologic conditions are similar.

Description of Study Area

Stump Spring and Hiko Springs are in Clark County, southern Nevada (fig. 1). The location of southern Nevada relative to the Pacific Ocean is such that a substantial amount of moisture from prevailing westerly winter storms is captured by orographic lifting associated with the intervening Sierra Nevada Mountains (Quiring, 1965). This capture, or "rain shadow," results in leeward storms of diminished moisture content. Nevertheless, these areally extensive low-pressure, low-intensity winter storms account for two-thirds to three-quarters of mean-annual precipitation (Quiring, 1965; Moreo and others, 2014). During summer months, monsoonal air flow from the south accounts for high-intensity, short-duration convective storms of limited areal extent. Mean-annual precipitation recorded in nearby Las Vegas was 106 mm from 1981 to 2010 (National Weather Service, 2018). Despite its proximity to the Pacific Ocean, the clear dry air of the study area attributed to the rain shadow effect results in large diurnal temperature fluctuations that are more continental than maritime in nature (Houghton and others, 1975). Mean-daily high air temperature ranges from about 14 °C during winter to 41 °C during summer, and mean-daily low air temperature ranges from about 4 °C during winter to 27 °C during summer (National Weather Service, 2018).

Snowmelt in the mountains is the primary source of groundwater recharge to adjacent valleys in southern Nevada. Snowmelt infiltrates the surface and increases the soil moisture. When soil water storage exceeds capacity, recharge is generated and percolation through the underlying bedrock proceeds at a rate determined by the hydraulic conductivity. Percolating subsurface water is captured as recharge to local perched aquifers, is intercepted and discharged at local springs, or travels through fractured bedrock to replenish aquifers that extend laterally into and beyond adjacent valleys. A secondary recharge mechanism is focused infiltration of ephemeral runoff resulting from episodic rainfall events (Stonestrom and others, 2003, 2007). Runoff concentrates in washes and quickly infiltrates poorly graded wash beds. Focused recharge generally accounts for only a small fraction of total recharge; however, this sporadic water source can be substantial in desert wash environments such as those found at Stump Spring and Hiko Springs.

Groundwater discharges naturally primarily in low areas of intermontaine basins by (1) spring and seep flow, (2) transpiration by local phreatophytes, and (3) evaporation from soil and open water. Actual evapotranspiration measurements from discharge areas typically include spring and seep flow because most of the discharged water infiltrates into the subsurface where ultimately it is transpired by phreatophytes; therefore, AET measurements are used to estimate groundwater discharge. Actual evapotranspiration is the combined process that transfers evaporated and transpired water from the land surface to the atmosphere. The Greek roots of the word phreatophyte are "well plant," meaning that these plants behave like natural wells accessing groundwater from the

saturated zone or the overlying capillary fringe (Meinzer, 1927). Phreatophytes rely on consistently available groundwater for their existence in the desert Southwest.

Stump Spring

Stump Spring is in an incised wash about 30 km south and downgradient from the Spring Mountains. Snowmelt in the Spring Mountains percolates through highly-fractured Paleozoic carbonate rock and replenishes aquifers beneath the adjacent valleys of Pahrump (which includes Stump Spring), Las Vegas, and Indian Springs (Maxey and Jameson, 1948; Malmberg, 1967; Winograd and Thordarson, 1975; Harrill, 1986; Fenelon and others, 2016) (fig. 1). The flow-path length from recharge areas in the Spring Mountains to the discharge area at Stump Spring is considered intermediate (Toth, 1963; Freeze and Cherry, 1979; Knochenmus and others, 2008, p. 37). The Stump Spring desert riparian area—described as an arroyo by Malmberg (1967)—is in an ephemeral riparian area, also called an xeroriparian area (Zaimes and others, 2007) (fig. 2*A*). Malmberg (1967) reported that the wash channel typically is dry except during and following large precipitation events.

Continuous (15-minute) discharge data have been collected at Stump Spring by the USGS since December 4, 2013 (USGS site 355906115492601). Discharge for the period of record (through September 15, 2019) was 0 m^3/s for about 95 percent of the record. Large flows (>1 m^3/s) in response to precipitation runoff events were recorded 10 times (fig. 2*B*). Smaller flows in response to recharge from the Spring Mountains occurred twice—from March 16, 2017, to May 17, 2017 (as much as 0.13 m^3/s), and from April 9, 2019, to July 17, 2019 (as much as 0.56 m^3/s). A substantially wetter-than-average snow year in the Spring Mountains during the winter of 2018–19 provided an opportunity to view evaporative stress (groundwater-level fluctuations in response to *GWET*) at this typically dry spring (fig. 2*C*). Spring discharge increases through each morning as recharge exceeds *GWET* and decreases in the afternoon through evening as phreatophytes withdraw groundwater and *GWET* exceeds recharge.

The BLM installed a groundwater monitoring well in 1997 (fig. 2*A*; USGS site 355941115490901). Groundwater levels in discharge areas of the western United States typically decline each growing season when phreatophytes withdraw groundwater and outflow from the aquifer exceeds inflow and rise after each growing season when phreatophytes are quiescent and inflow exceeds outflow (White, 1932; Laczniak and others, 1999; Fenelon and Moreo, 2002). For example, at Ash Meadows—a large regional groundwater discharge area about 65 km to the northwest—annual minimum depths-to-groundwater typically occurred during early spring and annual maximum depths-to-groundwater occurred during early autumn (Laczniak and others, 1999; Moreo and others, 2017). In contrast, the annual minimum depth-to-groundwater in Stump Spring well occurred during early summer and the annual maximum occurred during early winter—a lag of about 3 months compared to the typical example. Compared to the typical discharge-area example, the lagged water-level signal probably represents recharge processes to a greater degree than discharge because the relatively deep screened interval (36.4–37.2 m below land surface) may be partially isolated from relatively shallow root zones. Wells installed to monitor evaporative stress in discharge areas—such as those listed in Laczniak and others (1999, table 8)—typically are shallow (2–6 m) and are screened across the water table. The mean-annual groundwater-level fluctuation at Stump Spring well (0.61 m) was comparable to the low end of the range for those in Ash Meadows (0.64–3.11 m; Moreo and others, 2017). The water level rose by 2.27 m during December 17, 2004–August 29, 2005, in response to a wetter-than-average snow year in the Spring Mountains (2004–05). Annual mean groundwater levels declined from 7.56 m below land surface in 2005 to 8.56 m below land surface in 2017.

Hiko Springs

Hiko Springs, also considered a xeroriparian area, is in an incised wash on the southern end of the Newberry Mountains, approximately 10 km west of Laughlin, Nevada (fig. 1). This area in the Newberry Mountains is composed of Proterozoic intrusive and metamorphic rocks (Longwell and others, 1965). The source of groundwater recharge in this area likely is entirely derived from infiltration of ephemeral runoff resulting from episodic rainfall events because the surrounding mountains are low in elevation (<1,800 m) and receive little if any snow. It seems that Hiko Springs—which essentially is a series of ephemeral seeps—is fed by water flowing through the (probably) shallow alluvium on top of the Proterozoic basement rocks. Storm runoff focuses in upgradient channels, infiltrates into an interflow zone, and then discharges back through Hiko Springs downgradient along the channel as intermittent baseflow where the alluvium pinches out. This recharge mechanism can be highly variable from year to year. A concrete and earthen dam retention basin located about 5.5 km west of Laughlin captures excess storm runoff past the terminus of the wash that otherwise would drain directly to the Colorado River. Attempts to measure the spring discharge have been unsuccessful. Substantial flooding in September 2015 scoured the wash channel of vegetation and ripped out a flume and stilling well (B. Poff, Bureau of Land Management, written commun., 2019). Water-quality data including field parameters, the concentration of major ions, trace metals, nutrients, and the ratios of stable isotopes were collected at Hiko Springs from 2008 to 2010 (USGS site 351009114404201; Pavelko, 2014). No wells exist in the Hiko Springs drainage area for collection of groundwater-level data, and a shallow piezometer was not installed at or near Hiko Springs as part of the current study.

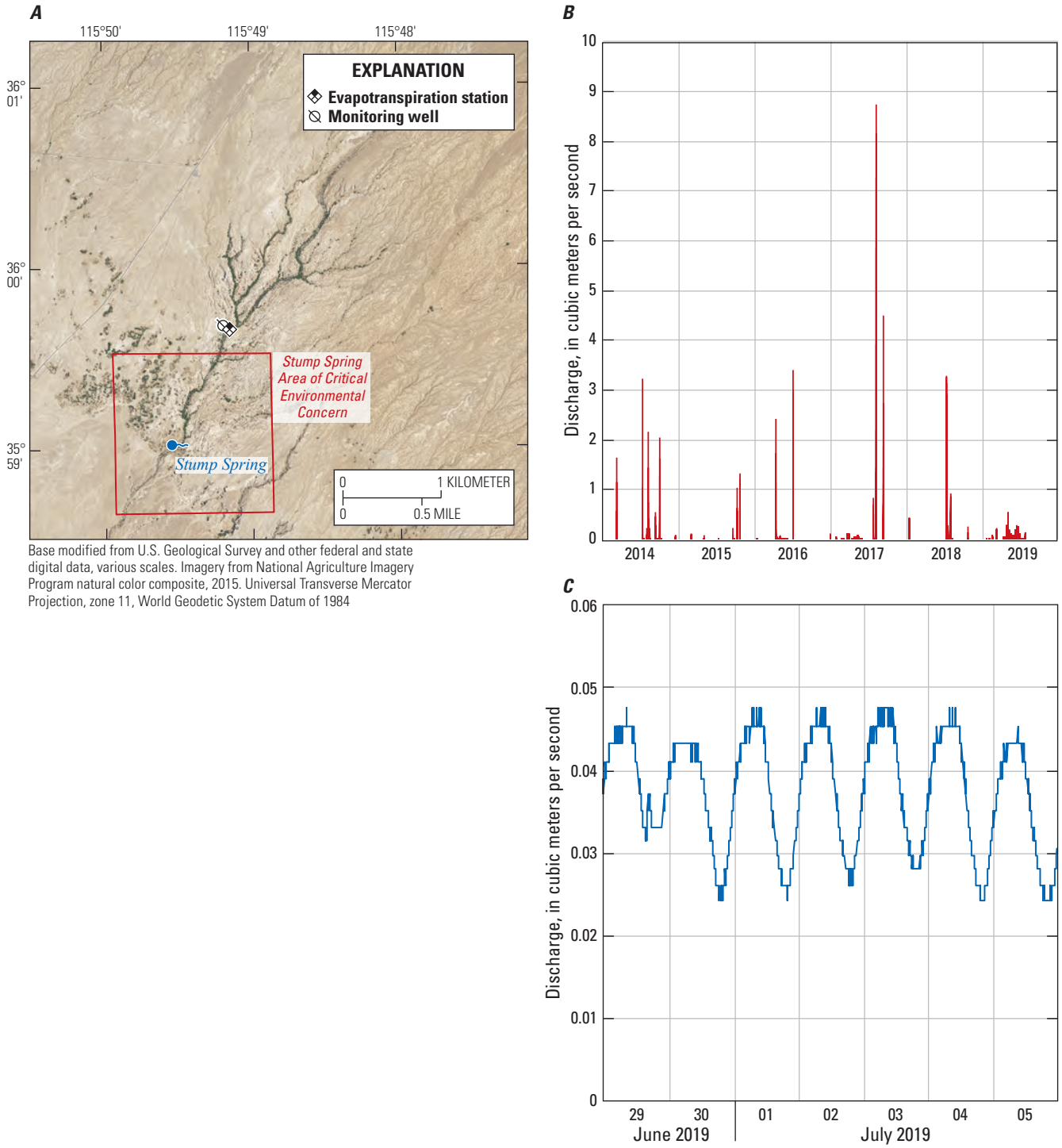

Base modified from U.S. Geological Survey and other federal and state digital data, various scales. Imagery from National Agriculture Imagery Program natural color composite, 2015. Universal Transverse Mercator Projection, zone 11, World Geodetic System Datum of 1984

Figure 2. Locations of spring, groundwater monitoring well, and eddy-covariance evapotranspiration station (*A*); and graphs showing spring discharges from January 1, 2014, to September 15, 2019 (*B*), and from June 29, 2019, to July 6, 2019 (*C*); at Stump Spring, Clark County, southern Nevada.

Study Sites

The primary criteria for determining suitable locations to measure continuous AET using standard sensors to apply the eddy-covariance method (eddy-covariance sensors) were accessibility and extensiveness of fetch. Fetch is the extent of uniform vegetative cover around the sensors (Stannard and others, 2013). The ideal site placement for an eddy-covariance station is one where the terrain surrounding the site is flat, and the fetch for the surface-of-interest (phreatophytes) is homogeneous and longer than the source area for measurements in all upwind directions. Because of the geometry of the riparian wash environments in this study, ideal site placements were not possible. The number of accessible sites with suitable fetch at Stump Spring and Hiko Springs was severely constrained by the long, narrow, sinuous nature of their riparian corridors (fig. 1). An accessible site with the greatest fetch in each area was selected and an eddy-covariance station including a precipitation gage was established. The station was operational from March 25, 2016, to March 6, 2017, at Stump Spring and then moved to Hiko Springs where it was operational from March 8, 2017, to December 7, 2018 (table 1). Fetch limitations at both sites required additional instrument-setup and data-processing considerations that are addressed throughout this report.

The eddy-covariance station was established 1.4 km upgradient from Stump Spring on top of a cut-bank in the wash overlooking the phreatophytic vegetation (table 1, figs. 2 and 3). The phreatophytes consisted primarily of western honey mesquite, a deciduous, thorny tree. Honey mesquite is a phreatophyte typically found in alkali sinks, washes, and dry lakes where plants have access to groundwater. General characteristics include an extensive root system with lateral roots and a taproot that commonly reaches depths of 12 m when subsurface water is available and leaf-drop that commonly occurs in November or December (Steinberg, 2001). Minor amounts of screwbean mesquite (*Prosopis pubescens* Benth.), tamarisk (*Tamarix L.*), fourwing saltbush [*Atriplex canescens* (Pursh) Nutt.], and shadscale [*Atriplex confertifolia* (Torr. & Frém) S. Watson] also were present. The mean height of the honey mesquite within the fetch area was about 4 m. The ecosystem was classified as mesquite/acacia (Heaton and others, 2011).

Following the measurements at Stump Spring, the eddy-covariance station was moved to a small (about 100-m) widening of the riparian corridor at Hiko Springs (table 1, fig. 4). The phreatophytes within the fetch area consisted primarily of shrubs with a mean height of about 1 m including desert baccharis (*Baccharis sergiloides* A. Gray), arrowweed [*Pluchea sericea* (Nutt.) Coville], and quailbush [*Atriplex lentiformis* (Torr.) S. Watson] (fig. 5). A perennial grass—alkali sacaton [*Sporobolus airoides* (Torr.) Torr.]—also was present. Screwbean mesquite, willow (*Salix* sp.), Fremont's cottonwood (*Populus fremontii* ssp. *fremontii*), common reed [*Phragmites australis* (Cav.) Trin. ex Steud.], Mexican rush [*Juncus balticus* ssp. *mexicanus* (Willd. ex Schult. & Schult. f.) Snogerup], and broadleaf cattail (*Typha latifolia* L.) were present outside of the fetch area but within the GDA (B. Poff and L. Kobelt, Bureau of Land Management, written commun., 2018). This ecosystem also was classified by Heaton and others (2011) as mesquite/acacia.

Table 1. Evapotranspiration station locations, periods of operation, and periods of reported measurements, Stump Spring and Hiko Springs, Clark County, Nevada, 2016–18.

[**U.S. Geological Survey site identification:** Unique identification number for site as stored in files and databases of the U.S. Geological Survey]

Site name	U.S. Geological Survey site identification	Latitude (decimal degrees)	Longitude (decimal degrees)	Elevation (meters)	Period of operation	Period of reported measurements
Stump Spring	355939115490901	35.9943	-115.8192	869	03-25-16 to 03-6-17	04-21-16 to 12-21-16
Hiko Springs	351010114403401	35.1695	-114.6761	556	03-08-17 to 12-07-18	04-11-17 to 12-04-18

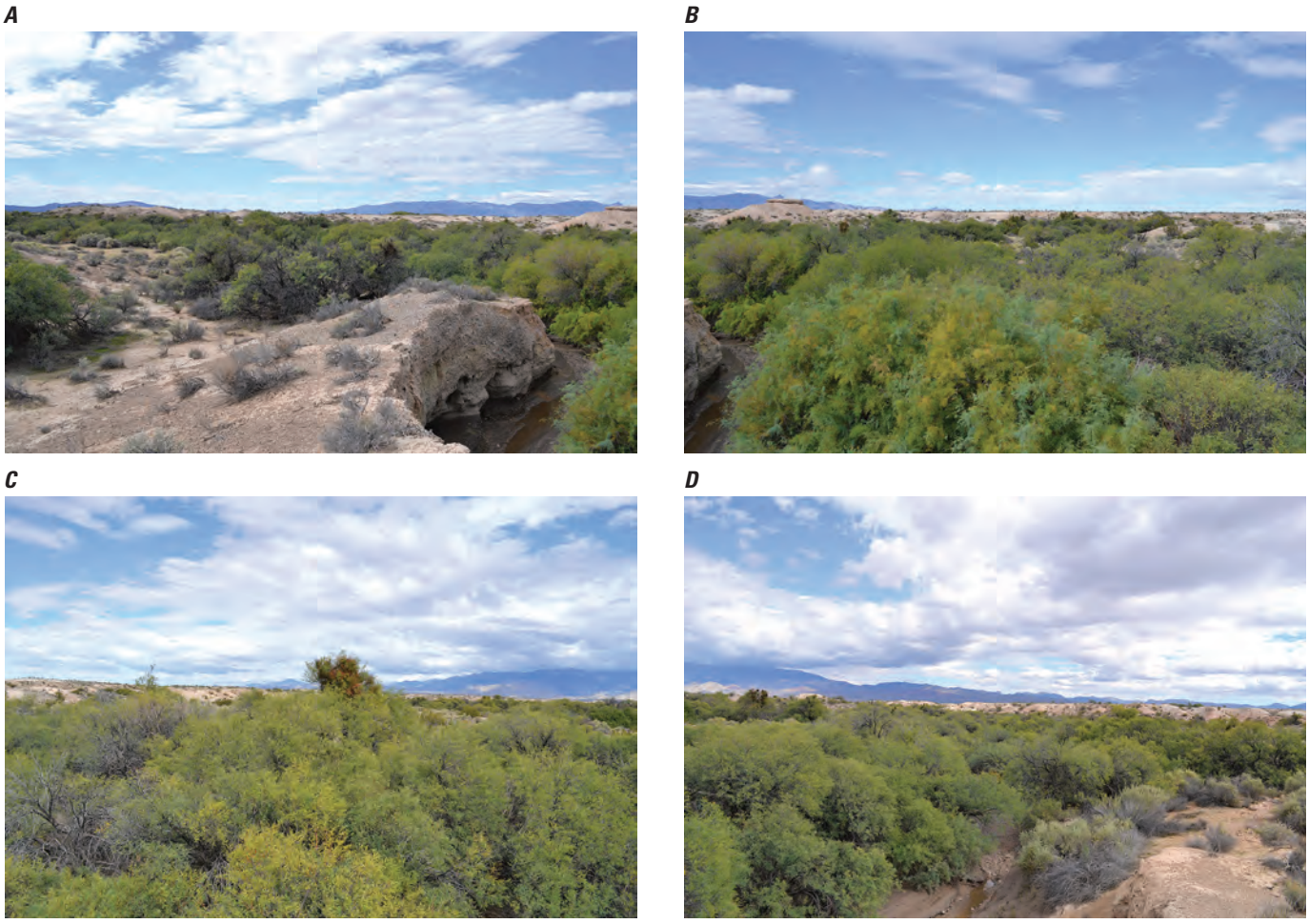

Figure 3. Photographs taken from eddy-covariance evapotranspiration station showing primarily honey mesquite within the fetch area to the southwest (*A*), west (*B*), north (*C*), and northeast (*D*), Stump Spring, Clark County, southern Nevada. Photographs by Michael. T. Moreo, U.S. Geological Survey, October 21, 2015.

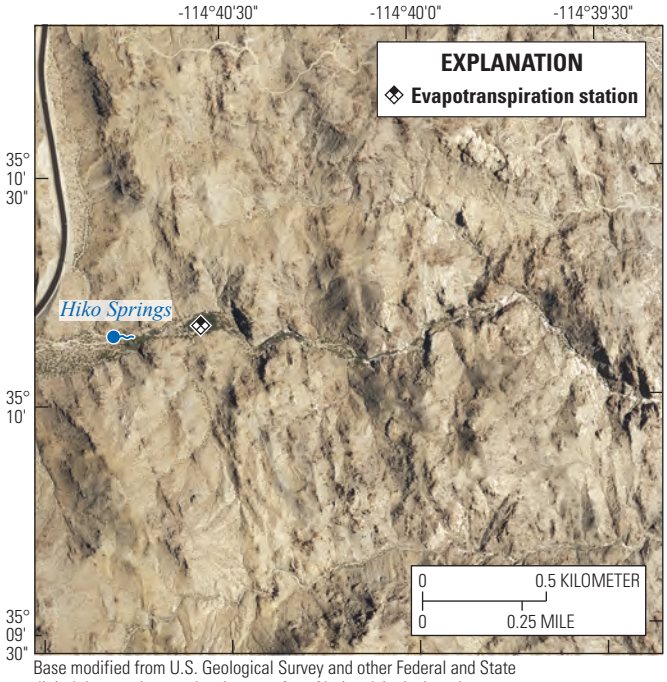

Base modified from U.S. Geological Survey and other Federal and State digital data, various scales. Imagery from National Agriculture Imagery Program natural color composite, 2015. Universal Transverse Mercator Projection, zone 11, World Geodetic System Datum of 1984

Figure 4. Locations of main spring orifice and eddy-covariance evapotranspiration station, Hiko Springs, Clark County, southern Nevada.

Figure 5. Looking north at eddy-covariance evapotranspiration station with primarily phreatophytes within the fetch area, Hiko Springs, Clark County, southern Nevada. Photograph by Michael. T. Moreo, U.S. Geological Survey, June 8, 2017.

Study Methods

Evapotranspiration is the process that transfers water from land surface to the atmosphere and occurs as evaporation (or sublimation when below freezing) from open water, soil, and plant canopies, and as transpiration from plants. Net radiation (R_n)—the difference between incoming and outgoing long-wave and shortwave radiation—is the primary driver of evapotranspiration processes. The largest component of R_n is radiative energy from the sun (incoming shortwave radiation). Net radiation is absorbed at the Earth's surface, and then is partitioned into energy that is transferred by heat conducted downward into the subsurface (G), by heat conduction or convection upward into the atmosphere (H), or is used to convert water from the solid or liquid phase to the vapor phase (LE) (Brutsaert, 1982). This partitioning process, which is based on the conservation of energy principles, can be expressed as:

$$R_n - G = LE + H, \quad (1)$$

where

R_n is net radiation,
G is soil-heat flux,
LE is latent-heat flux, and
H is sensible-heat flux.

All terms are in watts per square meter, and each term is positive during typical daytime conditions. R_n is positive when incoming long-wave and shortwave radiation exceeds outgoing long-wave and shortwave radiation, G is positive when heat moves from the surface into the subsurface, and LE and H are positive when water vapor and heat, respectively, move upward from the surface to the atmosphere. The left side of equation 1 represents the available energy and the right side represents the turbulent flux. Energy used for photosynthesis and energy stored as heat in short and sparse canopies are considered negligible for this study and are not accounted for in the energy-balance equation (Brutsaert, 1982; Wilson and others, 2002). A greater proportion of available energy is partitioned into H in arid environments where water supplies are limited; however, following precipitation events, a greater proportion of available energy is partitioned into LE.

Eddy-Covariance Evapotranspiration and Energy-Balance Measurements

Each study site was equipped with eddy-covariance and other sensors necessary to independently measure each major energy-balance component (eq. 1). Eddies are turbulent airflow caused by wind, surface roughness, and convective heat flow in the atmospheric surface layer (Swinbank, 1951; Brutsaert, 1982; Kaimal and Finnigan, 1994). Eddies transfer energy and mass between the land surface and atmosphere through a process referred to as turbulent energy exchange (Brutsaert, 1982). The eddy-covariance method represents the best available technology and is the most direct measure of turbulent energy exchange currently (2020) available (Baldocchi, 2003; Foken, 2008; Stannard and others, 2013). Fluxes of water vapor, heat, and other scalars such as carbon dioxide can be measured directly without the application of empirical constants (Foken, 2008). Evapotranspiration (positive LE) occurs when water vapor in upward-moving eddies is greater than in downward-moving eddies. LE is the product of the latent heat of vaporization of water (λ) and water-vapor flux density. The latent heat of vaporization, although slightly temperature-dependent, is nearly a constant. Water-vapor flux density is calculated as the covariance of instantaneous deviations from the time-averaged product of water-vapor density and vertical wind speed. LE can be expressed mathematically as:

$$LE = \lambda \overline{w' \rho_v'}, \quad (2)$$

where

λ is the latent heat of vaporization, in joules per gram;
w is the vertical component of wind speed, in meters per second; and
ρ_v is water-vapor density, in grams per cubic meter, where the overbar is the mean and the prime is the deviation from the mean over a 30-minute averaging period.

H is computed from temperature and vertical wind speed:

$$H = \rho_a C_p \overline{w' T_a'}, \quad (3)$$

where

ρ_a is air density, in kilograms per cubic meter;
C_p is specific heat of air at constant pressure, in joules per kilogram per degree Celsius; and
T_a is air temperature, in degrees Celsius, where the overbar is the mean and the prime is the deviation from the mean over a 30-minute averaging period.

Instrumentation

The eddy-covariance method uses fast-response sensors to measure rapid fluctuations in water-vapor density, wind-speed components, and air temperature to compute LE and H. Two specialized sensors were used—a krypton hygrometer (KH20) measured water-vapor density fluctuations, and a sonic anemometer (CSAT3) measured three-dimensional wind-vector and air-temperature fluctuations (table 2; fig. 6*A*). A krypton lamp in the KH20 sensor emits an ultraviolet radiation signal along an approximately 1-cm path open to the atmosphere. The signal is attenuated according to the Beer-Lambert law as water vapor absorbs specific frequencies of ultraviolet radiation. A voltage output proportional

Table 2. Instruments used to measure evapotranspiration, energy balance, and precipitation, Stump Spring and Hiko Springs, Clark County, southern Nevada, 2016–18.

Type of measurement	Company name	Model number and instrument
Turbulent flux/ Evapotranspiration	Campbell Scientific, Inc.	CSAT3 3-D sonic anemometer
		KH20 krypton hygrometer
Air temperature/ humidity	Rotronic	HC2S3 temperature/ humidity probe
Net radiation	Kipp & Zonen	NR-LITE2 net radiometer
Soil temperature	Campbell Scientific, Inc.	(2) TCAV averaging soil thermocouple probes
Soil moisture	Campbell Scientific, Inc.	CS616 water content reflectometer
Soil heat flux	Hukseflux	(2) HFP01 soil heat flux plates
Precipitation	NovaLynx	260-2510 standard rain gage

to the attenuated signal is recorded and related to water-vapor density by a regression function (Campbell Scientific, Inc., 2010a). The CSAT3 measures turbulent fluctuations of horizontal and vertical wind speed using three pairs of non-orthogonally oriented transducers to transmit and receive an ultrasonic signal. The Doppler effect relates the flight time of the signal to wind speed (Campbell Scientific, Inc., 2010b). An electronic datalogger (CR3000, Campbell Scientific, Inc.) received output from these sensors at a frequency of 10 hertz (Hz) (10 times per second). The centers of the KH2O and CSAT3 signal paths were separated by 10 cm horizontally and both sensors were positioned vertically. The CSAT3 was oriented to an azimuth of 270 degrees at both sites. The height of the paired sensors was 5.8 m above land surface at Stump Spring and 2 m above land surface at Hiko Springs. The orientation and positioning of the sensors were selected to minimize airflow disruptions that could be caused by the support structure and other sensors. The sensors also were positioned as low as possible to minimize the turbulent-flux source area and limit any potential contributions from non-phreatophytic vegetation, but still were high enough above the vegetation to capture well-mixed conditions and avoid measurement artifacts from underlying heterogeneities.

Net radiation was measured with a net radiometer (NR-LITE2) oriented to an azimuth of 180 degrees (table 2; fig. 6*B*). Radiometer heights above land surface were 2.9 m at Stump Spring and 2.4 m at Hiko Springs. Vegetation distribution at each site was patchy and heterogeneous on a local scale. The net radiometer height at each site was selected so the sensor's field-of-view would capture a representative ratio of vegetation to open ground. Stannard and others (1994) reported that reasonably accurate and consistent R_n data can be attained from stations with differing source areas (which is a function of sensor height above land surface) in areas of heterogeneous vegetation if care is taken during horizontal placement of the sensor. The source area for R_n measurements is a cosine-weighted average circular area with a radius of 10 times the sensor height above land surface (Campbell Scientific, Inc., 2010a). Net radiation data were corrected for sensitivity to wind speed as suggested by Campbell Scientific, Inc. (2010a). The source-area radius was 29 m at Stump Spring and 24 m at Hiko Springs.

Soil-heat flux was computed from data collected with two soil-heat flux plates (HFP01), four soil-temperature thermocouples (TCAV), and one water content reflectometer (CS616; table 2; fig. 6*C*). A set of one heat-flux plate and two thermocouples was installed in partial shade and the other set was installed in full sun. The soil-heat flux plates were placed at depths of 0.08 m below land surface and the soil-temperature thermocouples were placed at depths of 0.02 and 0.06 m below land surface. Heat flux was computed from the change in soil temperature and volumetric water content measured above each plate and added to the mean soil-heat flux measured across the plates (Campbell Scientific, Inc., 2012). Volumetric water content was computed using the standard calibration (Campbell Scientific, Inc., 2016). The source area for G measurements is small and limited to an area <1 m^2 at the sensors.

All instruments were calibrated by the manufacturer shortly before installation and recalibrated according to manufacturer guidelines. Each site was visited approximately monthly for data collection and site maintenance. Instruments were inspected and maintained according to manufacturer specifications. During each site visit, the NR-LITE2 and CSAT3 were checked for proper horizontal level and adjusted if necessary, and the NR-LITE2 and KH2O were cleaned with distilled water. Soil moisture and vegetation conditions were documented during each site visit.

Data Processing

Several standard corrections must be applied to raw eddy-covariance measurements to compensate for limitations in the eddy-covariance theory and equipment design. Raw 30-minute block-averaged covariances (eqs. 2 and 3) are computed from sampled 10-Hz data after filtering spikes (Højstrup, 1993) and

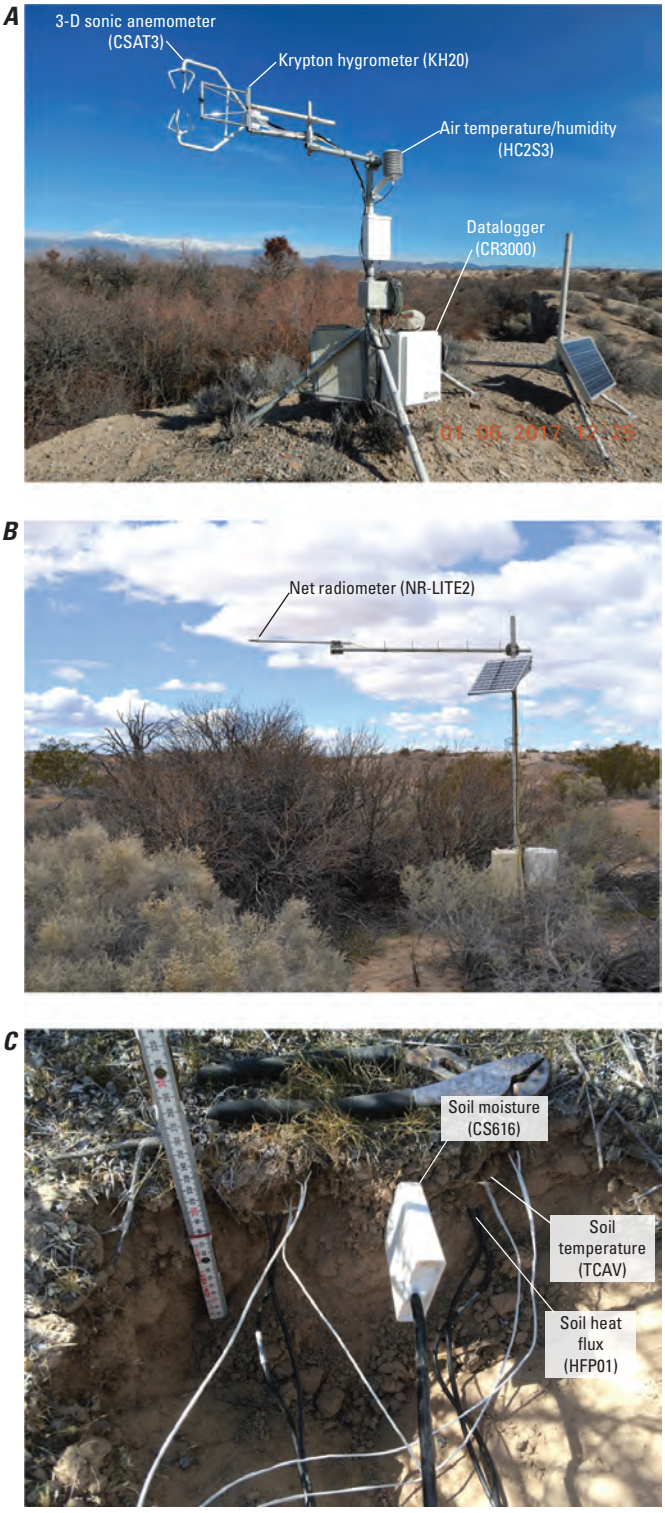

Figure 6. Eddy-covariance evapotranspiration station with snow-covered Spring Mountains in the background (*A*), net radiometer (*B*), and sensors used to compute soil-heat flux (*C*), Stump Spring, Clark County, southern Nevada. Photographs by Michael T. Moreo, U.S. Geological Survey, January 6, 2017 (*A*), March 30, 2016 (*B*), and April 8, 2016 (*C*).

removing any lag between CSAT3 and KH2O signal outputs. To correct errors associated with small misalignments of the CSAT3, raw covariances are two-dimensionally rotated to align with the mean streamlines of airflow, which forces the mean vertical and crosswind velocities to zero (Kaimal and Finnigan, 1994). Frequency response corrections were applied that compensate for the inability of eddy-covariance sensors to measure contributions from the largest (>1 km) and smallest (<10 cm) eddies due to averaging time and sensor geometry such as path-length averaging and sensor separation (Moore, 1986). The contribution to non-zero average vertical wind speed caused by variations in the density of rising and falling air is corrected following Webb and others (1980). The attenuation of the KH20 signal caused by oxygen in the approximately 1-cm signal path, which is proportional to *H*, is corrected as suggested by Tanner and Greene (1989). Additionally, *H* is corrected for air density and sound-path deflection of sonic-derived temperatures (Schotanus and others, 1983). EdiRe software (Clement, 2012) was used to post-process the 10-Hz data and apply the preceding corrections.

Gap-Filling Poor-Quality, Unrepresentative, or Missing Data

Following post-processing, time-series *LE* and *H* data received additional filtering to remove poor-quality data resulting primarily from precipitation events and unrepresentative wind directions. Spurious spikes in high-frequency *LE* and *H* measurements can occur for several reasons, but the most common reason in this study was from precipitation. Latent-heat-flux data spiked during precipitation events because water accumulation on the KH2O attenuated the millivolt output signal. Additionally, random spikes in *LE* and *H* data less than -150 W/m^2 and greater than (>) 700 W/m^2 were considered physically improbable and were filtered (Law and others, 2005). Poor-quality data resulting from precipitation and random data spikes accounted for the removal of about 1 percent of *LE* and *H* data at both sites.

A filter was applied to the Stump Spring dataset to remove *LE* and *H* data when the wind originated from directions representing primarily xerophytes. As stated previously (see section, "Study Sites"), the eddy-covariance station was established on top of a cut-bank in the wash where about two-thirds of the fetch was dominated by phreatophytes in the wash and one-third was dominated by xerophytes outside the wash. When the wind originated from azimuths from 80 to 210 degrees, airflow past the sensors equilibrated to upland xerophytes and, therefore, *LE* and *H* data associated with those wind directions were removed. This filter resulted in the removal of about 33 percent of daytime *LE* and *H* data. Nighttime *LE* and *H* data were not filtered because minimal energy is available to drive evaporative processes at night. Gaps also resulted from missing data. A malfunction of the CSAT3 resulted in about 6 percent of *LE* and *H* data missing from the Stump Spring dataset (14 days,

October 24–November 7, 2016), and no data were available for 28 days (July 19–August 16, 2018) accounting for about 5 percent of the Hiko Springs dataset.

Data gaps resulting from filter procedures and missing data were filled using estimated values. The estimation method depended on gap length. Any gaps in *LE* or *H* data occurring for <2 hours were filled by averaging values measured before and after the gap period. Gaps >2 hours and <1 week were filled using a multivariate regression model at a 30-minute time step (SeriesSEE; Halford and others, 2012). Data gaps larger than 1 week were simulated as a daily mean timestep.

The water-level model utility in SeriesSEE (Halford and others, 2012, p. 4–11) was used to simulate and gap-fill AET data (Garcia and others, 2015, p. 18–19; Smith and others, 2017, p. 9–11). Continuous time-series data (R_n, *H*, *LE*, *G*, and precipitation) were used to simulate turbulent fluxes (*H* and *LE*). Model components including raw time-series and multiple moving-average transformations (30 minutes to days) of continuous time-series data were automatically adjusted in magnitude and phase to simulate different signal frequencies. Turbulent fluxes were simulated as the summation of transformed and adjusted time-series data. Gaps in *H* were modeled using moving averages of R_n. Gaps in *LE* were modeled using moving averages of R_n and *H*. Gaps in *LE* coinciding with precipitation were modeled with a gamma transform of continuous precipitation data to improve goodness-of-fit (Halford and others, 2012). The gamma transform was used to simulate the attenuation, intensity, and length of *LE* fluxes after precipitation events (Garcia and others, 2015). The water-level model utility in SeriesSEE uses Parameter ESTimation (PEST, Doherty, 2010a, 2010b; Halford and others, 2012) to automatically adjust (or calibrate) the magnitude and phase of the model components to minimize the error between the simulated and measured fluxes prior and (or) subsequent to data gaps.

Flux data from the closest concurrently operating eddy-covariance stations were used as model inputs to gap-fill the two extended periods of missing data. The 14-day gap in *LE* and *H* data for Stump Spring (October 24, 2016–November 7, 2016) was simulated with fluxes from an eddy-covariance station located about 130 km northwest of Stump Spring (USGS site 364555117412401; Moreo and others, 2018). The 28-day period for Hiko Springs (July 19, 2018–August 16, 2018) when all data (R_n, *H, LE,* and *G*) were lost was simulated using previously unpublished data (acquired October 2018) from a site about 170 km west-northwest of Hiko Springs. The sensor array and data-processing methods for this eddy-covariance station (USGS site 355846116160401) were identical to those reported for the current study.

Goodness-of-fit for each gap-filled estimate is reported, and all gap-filling simulations were guided with a maximum root-mean-squared (RMS) error of 20 W/m^2 (Smith and others, 2020). The mean gap-filled *LE* at Stump Spring was 45.6 W/m^2 with an RMS error of 10.1 W/m^2, and the mean gap-filled *LE* at Hiko Springs was 26.6 W/m^2 with an RMS error of 5.7 W/m^2. An inventory of gap-filling procedures, goodness-of-fit model results, and previously unpublished data is given in Smith and others (2020).

All 30-minute data for the period of reported measurements (table 1) are archived in the USGS National Water Information System (U.S. Geological Survey, 2019). Datasets can be accessed either by searching the site identification numbers (table 1) or through the USGS Nevada Water Science Center evapotranspiration web portal. Additionally, daily values were aggregated and plotted from 30-minute gap-filled data and compiled in an electronic spreadsheet distributed with this report (appendix 1).

Energy-Balance Closure and Correction

The computed energy-balance ratio (*EBR*) was used to assess the accuracy of corrected and gap-filled *LE* and *H* data and to apply an additional correction based on energy imbalances. The energy balance is based on conservation of energy principles and the degree to which energy-balance closure is achieved is quantified by the *EBR*; notwithstanding this, good energy-balance closure can result from offsetting erroneous measurements (Wilson and others, 2002):

$$EBR = \frac{\sum LE + \sum H}{\sum R_n - \sum G} \quad (4)$$

Ideally, if all energy fluxes are measured accurately (within the limits of measurement accuracy), then the *EBR* will equal unity. In reality, eddy-covariance turbulent flux (eq. 4 numerator) is consistently less than the available energy (eq. 4 denominator). Wilson and others (2002) studied the results of other investigators and report *EBR* values ranging from 0.39 to 1.69 for 50 site-years of data at 22 eddy-covariance sites. Typical *EBR* values range from 0.6 to 1.0, but most frequently range from 0.7 to 0.8, thus implying that on average 70–80 percent of available energy is accounted for by their turbulent-flux measurements (Twine and others, 2000; Wilson and others, 2002; Foken, 2008).

Resolving the so-called energy-balance closure problem—balancing the turbulent energy against independently measured available energy—is an active area of research. Various theories have been advanced by the scientific community to explain this discrepancy (Twine and others, 2000; Wilson and others, 2002; Foken, 2008; Foken and others, 2012; Leuning and others, 2012), but currently (2020) there is no consensus. A commonly applied remedy to close the energy balance is to force closure while maintaining the ratio between *LE* and *H* (the Bowen ratio) (Twine and others, 2000; Foken and others, 2012). To apply this method, an investigator must have confidence that (1) available energy measurements are reasonably accurate, and (2) the "missing" turbulent flux can be estimated by assuming that the missing *LE* and *H* are in proportion to the Bowen ratio (scalar similarity). However, there is evidence that this technique may not

be applicable in all situations, as a large part of the unclosed energy budget may be related to *H* (Foken and others, 2012; Moreo and others, 2017, p. 27).

Given the state of knowledge, the decision whether or not to force closure can be considered subjective. For the current study, energy imbalances were corrected, and uncertainties were estimated as described in Moreo and Swancar (2013, p. 25–29), Garcia and others (2015, p. 38), Berger and others (2016, p. 51–52), and Smith and others (2017, p. 11–12). Energy-imbalanced *LE* and *H* were assumed to represent the probable minima. Probable maxima were computed by adjusting *LE* and *H* upward to achieve energy-balance closure while maintaining consistency with the Bowen ratio. The best estimate of *LE* and *H* for the current study was assumed to be the mean of the probable minimum and maximum at each site. Uncertainty was estimated as the difference between the best estimate and the probable minimum/maximum plus uncertainties associated with gap-filling. This non-standard correction is applied only to growing season AET sums given in this report and is not applied to published daily or sub-daily data. This method was developed by the Nevada USGS and used when the cause or causes of energy-balance deficiencies cannot be determined because they are considered unbiased.

Turbulent-Flux Source Area

The turbulent-flux source area is the area upwind of the eddy-covariance sensors from which the measured variables (*LE* and *H*) originate. An estimate of the turbulent-flux source area is important to characterize the vegetation contributing to the measured fluxes. The turbulent-flux source area is dependent upon the sensor height, surface roughness, and atmospheric stability. Lower eddy-covariance sensor heights, rougher surfaces, and unstable atmospheric conditions (H >0) all reduce the turbulent-flux source area (Campbell and Norman, 1998). The cumulative normalized contribution to the measured turbulent flux (cumulative normalized flux, or CNF) increases with distance from the sensors (Schuepp and others, 1990). The relative contribution of turbulent flux (also called the footprint) is zero at the sensor location, increases rapidly to a maximum at a relatively short distance upwind of the sensors, then decreases asymptotically with increasing distance from the sensors (Moreo and others, 2007, fig. 8). An analytical model in the EdiRe processing program (Clement, 2012; Kormann and Meixner, 2001) was used to quantify the CNF at 25-, 50-, 75-, 100-, 200-, and 300-m distances upwind of the eddy-covariance sensors for periods when available energy was >0 W/m^2. Periods where the available energy was < 0 W/m^2 (typically nighttime) were excluded from this analysis because the energy to drive evaporative processes is minimal. The CNF mathematically extends to infinity, but because no measured surface is infinite, 50-, 75-, and 90-percent source areas contributing to a point flux measurement often are considered (Rannik and others, 2012). A 90-percent source area is used for the current study. Growing season CNF was computed as the median of 30-minute CNF means.

Precipitation Measurements

Precipitation data were collected at each study site with a National Weather Service-style standard non-recording precipitation gage. A funnel situated on top of the 20.3-cm diameter gage directed rain into a 5.1-cm diameter measuring tube (snowfall was not observed during the current study). Precipitation in the measuring tube was determined during monthly site visits using a measuring stick with a resolution of 0.25 mm. The measuring tube was then wiped clean with a paper towel and 50 mL of mineral oil was added to prevent the evaporative loss of precipitation that accumulated between monthly readings. Care was taken to add the mineral oil only to the bottom of the measuring tube using a pipette to ensure an accurate depth reading. Any mineral oil/water mixture adhering to the measuring stick after monthly readings was swiped back into the measuring tube. Corrections for gage-catch deficiencies follow those developed by Yang and others (1998) and reported in Moreo and others (2017, p. 16–17). Precipitation uncertainty is estimated as 2 percent (Garcia and others, 2015).

Determination of Groundwater Discharge Rates

The primary water sources contributing to AET were groundwater and precipitation. Actual evapotranspiration measured using eddy-covariance sensors does not differentiate between water sources; therefore, water sources other than groundwater need to be accounted for and subtracted from AET measurements. Groundwater discharge by evapotranspiration was computed using the following equation:

$$GWET = AET - P, \tag{5}$$

where

GWET is groundwater discharge by evapotranspiration,
AET is actual evapotranspiration, and
P is precipitation.

All terms are in millimeters per year. The effect of antecedent soil moisture on computed *GWET* was reduced to negligible levels using volumetric soil-water content data in conjunction with field observations to approximate growing-season lengths and determine analysis periods. For example, honey mesquite leaf-out was observed at Stump Spring from early-to-mid April 2016 and leaf-drop was observed from mid-to-late December 2016. An analysis period from April 21 to December 21, 2016, was selected based on these growing-season observations and the similarity of soil-water content at the beginning and end of each analysis period. The uncertainty of *GWET* was estimated using standard error-propagation techniques (Taylor, 1997; Lee and Swancar, 1997).

A secondary water source contributing to *AET* is flood runoff from excess precipitation. Flood runoff through the washes is a water source that originated outside of but moved into the turbulent-flux source area. The only known runoff event occurred at Stump Spring from July 1, 2016, at 7:30 a.m. to July 2, 2016, at 1:45 a.m. Discharge peaked at 2.34 ft^3/s on July 1, 2016, at 9:00 a.m. Peak *AET* on July 1 was about 3 times greater than previous days and receded in subsequent days. There are two components to this runoff event to consider—surface wetting and infiltration and subsequent percolation into the root zone. The contribution to *AET* from surface wetting is considered negligible because the wash channel where the flow occurred accounts for only a small part the eddy-covariance source area, and like the rest of the source area, the surface of the wash would have been wet from direct rain even with no flow. The volume of water that infiltrated and percolated into the root zone, and was consumed by the honey mesquite, was not accounted for. Honey mesquite is considered a facultative phreatophyte, meaning that it has the ability to use groundwater both in the unsaturated and saturated zones. Moreo and others (2017) reported, based on isotopic analyses, that water in the unsaturated zone is used preferentially by honey mesquite over water in the saturated zone. White (1932) reported the cessation of groundwater uptake from the saturated zone by facultative phreatophytes following precipitation events. Whether these processes offset each other at a 1:1 ratio is not known. As stated previously (see section, "Description of Study Area"), shallow aquifers in the area are recharged primarily by snowmelt in the Spring Mountains, but recharge to these aquifers also is supplemented by focused infiltration of ephemeral runoff in washes due to episodic precipitation events. Both of these water sources are required to sustain the extent, health, and vigor of mesquite in the study area observed during the study period.

Delineation of Groundwater Discharge Areas and Calculation of Vegetation Indexes

Groundwater discharge area boundaries typically are delineated by mapping the outer extent of naturally occurring phreatophytes in the area of interest (Smith and others, 2007). The GDAs for Stump Spring and Hiko Springs were mapped by visual interpretation of 2015 1-m resolution National Agriculture Imagery Program (NAIP) aerial imagery (U.S. Department of Agriculture, 2012). The natural drainage area tributary to Stump Spring was mapped from the southern extent of the ACEC boundary to the northeast following the visible extent of phreatophytes and landforms in the NAIP imagery. The delineation traced tributaries up-channel to the last large visible mesquite (>5 m on any axis). A second GDA defined by the ACEC boundary included a part of the natural drainage and also included vegetation (mesquite) found outside the natural drainage primarily in a sand-dune environment to the northwest of Stump Spring (fig. 2). The GDA for Hiko Springs followed the visible extent of phreatophytes within the incised wash from approximately 430 m west to 1,800 m east-southeast of the evapotranspiration station (fig. 4). These points were identified during field reconnaissance with the BLM in November 2015.

Many studies in Nevada and elsewhere have shown strong correlations between *GWET* and various vegetation indexes (VIs). The rate of *GWET* increases as VI values increase. A VI is a dimensionless, radiometric measure that functions as an indicator of the relative abundance and activity of green vegetation, percentage of green cover, chlorophyll content, green biomass, and absorbed photosynthetically active radiation (Jensen, 2000). For the current study, vegetation within each GDA was characterized using a Normalized Difference Vegetation Index (NDVI; Rouse and others, 1974). The NDVI was calculated from 1.84-m resolution WorldView-2 (WV2) images using the red and NIR1 bands (DigitalGlobe, 2010). The image dates were June 29, 2017 (Stump Spring), and May 11, 2016 (Hiko Springs). Native NDVI values range from -1 to 1. Values from 0 to -1 were excluded from the datasets because negative NDVI values typically represent non-vegetated areas (Garcia and others, 2015). The remaining NDVI values were rescaled (1 to 99) and binned by integer.

Vegetation was defined further at Stump Spring using a supervised classification to differentiate healthy, phreatophytic vegetation from xeric vegetation and bare ground. The classification was created by delineating 30 training locations identifying bare ground and vegetation within and near the Stump Spring GDA and ACEC. Areas of xeric vegetation and shadow associated with large mesquite were included in the bare ground training classes. The training locations were passed through a maximum likelihood supervised classification based on the 4-band NAIP imagery (Richards and Jia, 1999). No error analysis was done on the classification. The WV2 NDVI image was resampled from 1.84 to 1 m, and the extent of phreatophytic vegetation determined by the classification was used to determine vegetated NDVI values and estimate canopy cover. This classification was not done at Hiko Springs because the vegetation distribution changed between the 2015 NAIP and 2016 WV2 images. The wash channel was scoured by a flooding event in September 2015, resulting in a 14-percent decrease in vegetation. Therefore, the GDA at Hiko Springs required additional refinement by visually excluding bare ground areas identified using the WV2 imagery.

Groundwater Discharge by Evapotranspiration

Actual evapotranspiration increased through the spring, peaked during early summer, and declined through the autumn at both sites (figs. 7*A* and 7*C*). This cycle generally follows the sinusoidal seasonal pattern of R_n (figs. 7*B* and 7*D*). Spikes following precipitation events are superimposed on the pronounced seasonal *AET* pattern. The seasonal increase

and decrease in *AET* is indicative of a consistent and readily available water source that is independent of sporadic rainfall events. Correlative analyses of *AET* versus R_n indicate that the best coefficients of determination (r^2) were for Stump Spring in 2016 ($r^2 = 0.60$, precipitation = 52 mm) and Hiko Springs in 2017 ($r^2 = 0.57$, precipitation = 53 mm). The correlation between *AET* and R_n decreased for Hiko Springs in 2018 ($r^2 = 0.33$, precipitation = 81 mm) because precipitation increased by 53 percent, introducing additional scatter into the relation. For comparison, a similar analysis was done for 3 years of data from an eddy-covariance station located about 160 km northwest of Las Vegas in an area with a deep saturated zone (about 110 m; Moreo and others, 2017, 2018). In this case—where *GWET* = 0—the correlation between *AET* and R_n was very weak (mean $r^2 = 0.03$) for 3 growing seasons (2012, 2013, 2015). The good relations between *AET* and R_n for the current study strongly indicate the presence and use of shallow groundwater by phreatophytes.

The *EBR* values computed for Stump Spring (0.78) and Hiko Springs (2017 = 0.74, 2018 = 0.73) (table 3) were similar to the average for previous studies and indicate acceptable accuracy for turbulent-flux and available-energy measurements (see section, "Energy-Balance Closure and Correction"). Corrections for energy-balance-closure deficiencies increased measured *AET* at Stump Spring (14.3 percent) and Hiko Springs (2017 = 17.6 percent; 2018 = 18.6 percent).

Measured and corrected *AET* and *P,* and computed *GWET* and uncertainties are provided in table 4. The mean daily corrected *AET* rate for Stump Spring (1.19 mm/d, n = 244) was about 65 percent greater than for Hiko Springs (2017 = 0.73 mm/d, n = 241; 2018 = 0.71 mm/d, n = 249). Measured *P* corrected for gage-catch deficiencies increased *P* by an average of 6.6 percent at Stump Spring and 5.5 percent at Hiko Springs. The mean daily *P* rate at Stump Spring (0.21 mm/d) was similar to Hiko Springs in 2017 (0.22 mm/d) and about 31 percent less than at Hiko Springs in 2018 (0.32 mm/d). Computed *GWET* at Stump Spring (0.98 mm/d) was about twice as great as at Hiko Springs (2017 = 0.51 mm/d, 2018 = 0.39 mm/d). Site-scale *GWET* rates computed at Stump Spring (239 ±45 mm/yr) and Hiko Springs (2017 = 122 ±26 mm/yr, 2018 = 97 ±29 mm/yr) were well above estimated uncertainties, which indicates that *GWET* was >0 mm/yr.

Site-Scale Turbulent-Flux Source Area and Normalized Difference Vegetation Index Estimates

Turbulent-flux source area and footprint estimates represented by the CNF are provided in table 5. Assuming a 90-percent source area, 90 percent of the CNF at Stump Spring originated within 200 m of the eddy-covariance station. This source-area analysis excludes azimuths from 80 to 210 degrees as airflow originating from those directions equilibrated mostly to upland xerophytes, which was not representative of the phreatophytes in and adjacent to the wash (see section, "Gap-Filling Poor-Quality, Unrepresentative, or Missing Data"). Distances of 50, 100, and 200 m representing source areas upwind of the station are shown in figure 8*A*. The CNF distribution (the turbulent-flux footprint) indicates that about two-thirds of the CNF at 200 m originated within 50 m of the Stump Spring station. The turbulent-flux footprint at Hiko Springs was substantially smaller than the footprint at Stump Spring primarily because the instrument height at Hiko Springs was relatively low (2 m) compared to the mean vegetation height (1 m). About 92 percent of the CNF at Hiko Springs originated within 50 m of the eddy-covariance station (table 5, fig. 9*A*).

Site-scale NDVI was computed by weighting and averaging scaled NDVI according to CNF estimates given in table 5. Footprint-weighted-mean NDVI estimates were used to determine relations between NDVI datasets and computed *GWET*. Results of the vegetation classification and NDVI distribution at the Stump Spring eddy-covariance site calculated from NAIP and WV2 imagery are shown in figures 8*B* and 8*C*, respectively. About 67 percent of the area within 50 m of the station (excluding azimuths from 80 to 210 degrees) was phreatophytes (primarily honey mesquite), with a mean NDVI of 28.6 (table 6). The percentage of vegetation-to-bare ground decreased as the distance from the station increased. The mean NDVI for each turbulent-flux source-area distance in table 6 also decreased with increasing distance from the station. The mean NDVI for each turbulent-flux source-area distance was weighted based on the footprint contribution. The resulting footprint-weighted mean NDVI estimate was 26.7. Canopy cover was estimated at about 50 percent based on the ratio of vegetated to total pixels.

The footprint-weighted mean NDVI at Hiko Springs (0–25 m = 13.0; 25–50 m = 16.6; footprint-weighted mean = 13.5) was further refined based on wind direction because the NDVI distribution was heterogeneous around the eddy-covariance station (fig. 9*B*). Thirty-minute wind direction, measured-*AET*, and available-energy data were binned according to a 16-point compass rose and aggregated generally to the four cardinal compass directions. The first analysis considers daytime and nighttime combined data (24-hour data) and the second analysis considers daytime data only (periods when R_n-G >0 W/m^2; table 7). The greatest proportion of 24-hour wind was from the west (54 percent) followed by from the east (33 percent); however, measured *AET* was substantially less from the west (39 mm, 14 percent of total measured *AET*) than from the east (188 mm, 69 percent of total measured *AET*). Compared to 24-hour data, the proportion of daytime wind from the west decreased from 54 to 18 percent and the proportion of daytime wind from the east increased from 33 to 64 percent. These results indicate that the wind direction was strongly diurnal—wind was primarily from the west at night and from the east during the day. The measured *AET* rate for 24-hour data (273 mm/yr) was only 9 mm/yr greater than for daytime data (264 mm/yr), indicating that 96.6 percent of measured *AET* occurred during the day. Accordingly, the footprint-weighted mean NDVI was adjusted downward from

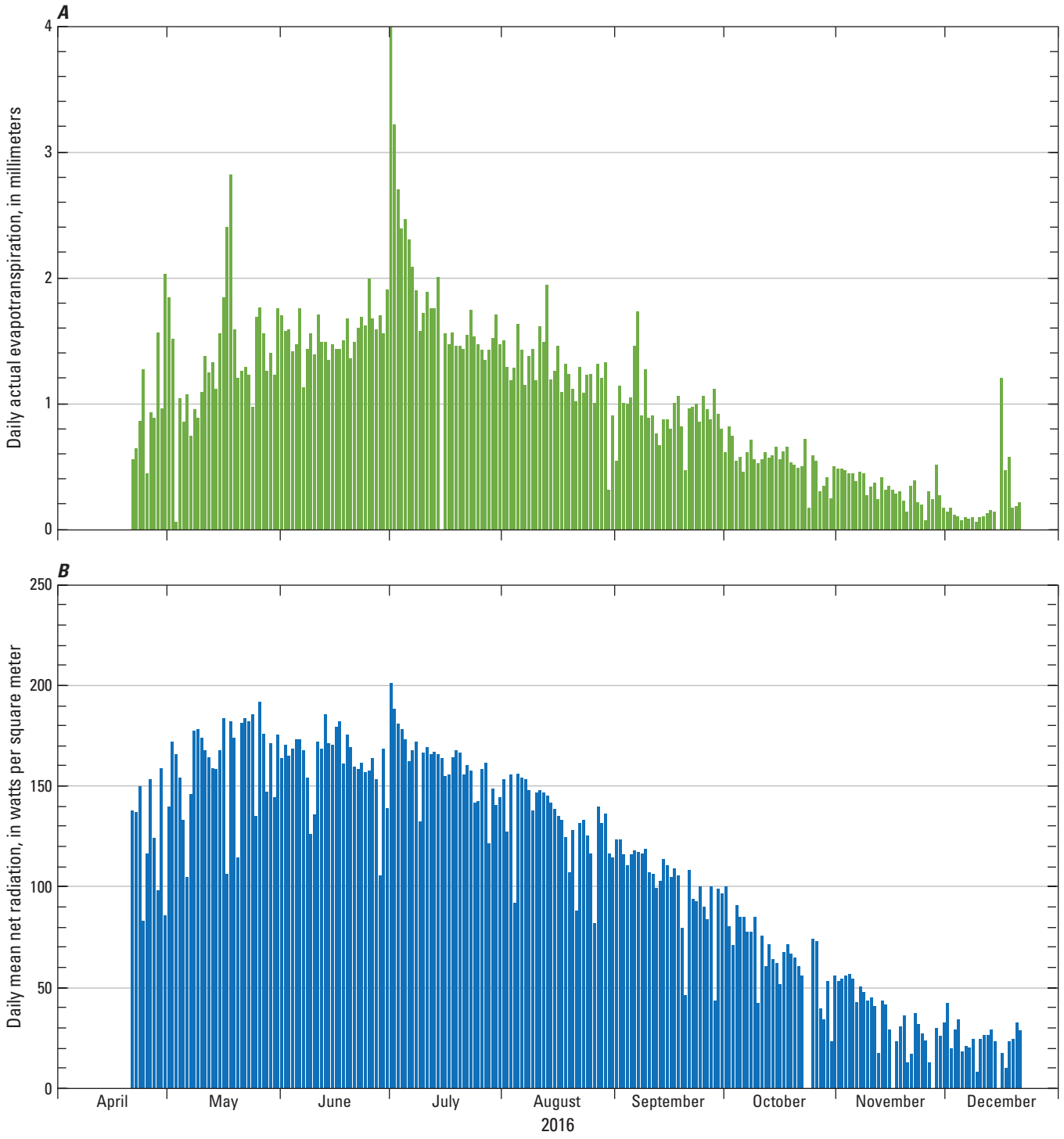

Figure 7. Daily actual evapotranspiration (*A*) and daily mean net radiation (*B*) measured at Stump Spring, and daily actual evapotranspiration (*C*) and daily mean net radiation (*D*) measured at Hiko Springs, Clark County, southern Nevada, 2016–18.

13.5 to 13.0 based on daytime winds. The adjustment was downward because the footprint-weighted mean NDVI on the east side of the station (primarily within 25 m) where daytime winds were dominant was about one-half of the mean NDVI on the west side. This additional step, to refine the footprint-weighted mean NDVI based on daytime wind direction, was considered questionable at Stump Spring and not done because of the amount of filtered or missing daytime data (40 percent) and highly complex fetch. The footprint and daytime-wind-direction weighted mean NDVI at Hiko Springs (13.0) was about one-half of the footprint-weighted mean NDVI computed at Stump Spring (26.7).

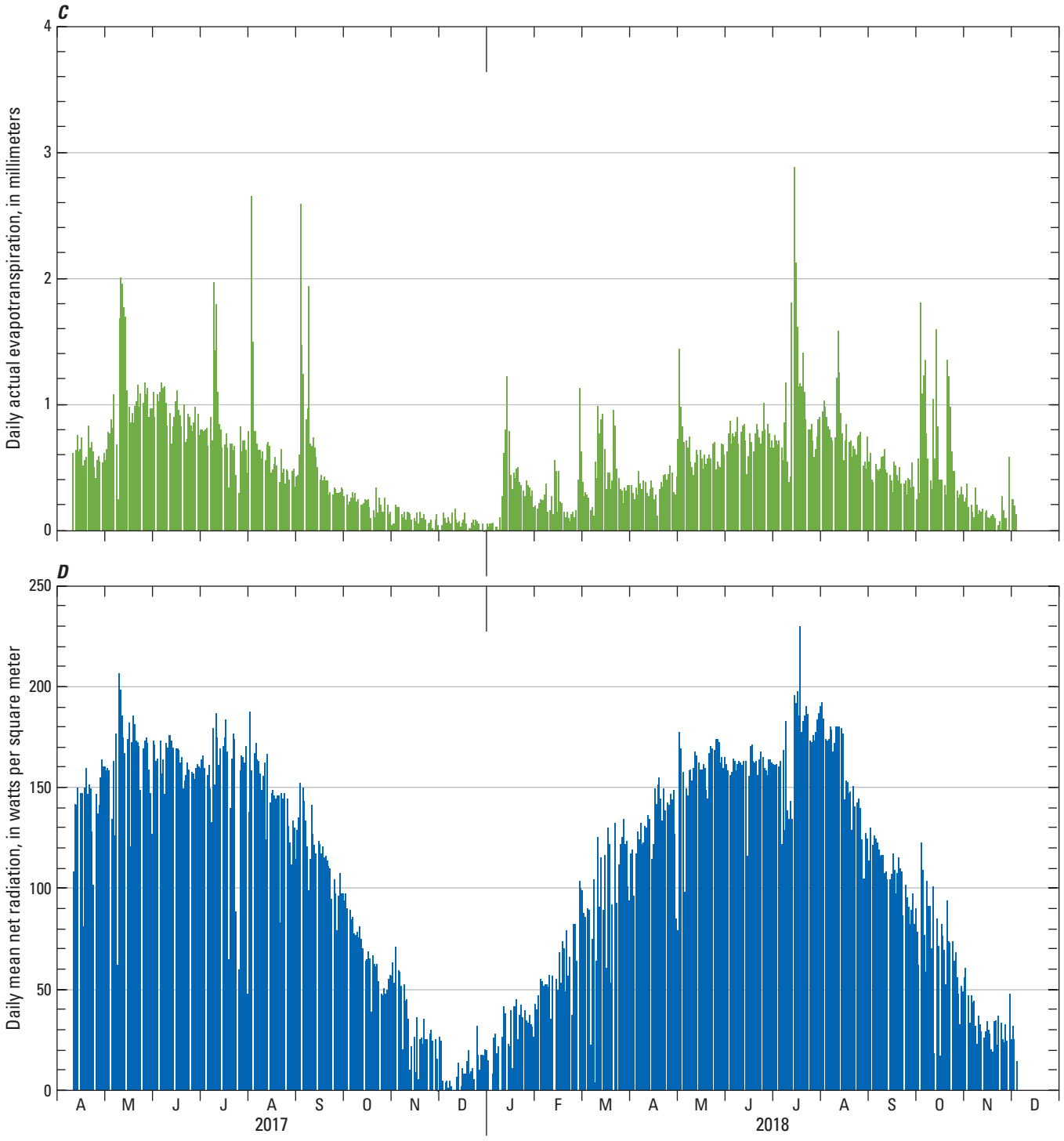

Figure 7. —Continued

Table 3. Mean daily energy-balance measurements and energy-balance ratios, Stump Spring and Hiko Springs, Clark County, southern Nevada, 2016–18.

[R_n: Net radiation. ***G***: Soil-heat flux. **Available energy**: Computed as R_n - G. ***LE***: Latent-heat flux. ***H***: Sensible-heat flux. **Turbulent flux**: Computed as *LE* + *H*. **Bowen ratio**: Computed as *H* divided by *LE*. ***EBR***: Energy-balance ratio, computed as turbulent flux divided by available energy (eq. 4). **Abbreviation:** W/m², watts per square meter]

Site name	Analysis period	R_n (W/m²)	*G* (W/m²)	Available energy (W/m²)	*LE* (W/m²)	*H* (W/m²)	Turbulent flux (W/m²)	Bowen ratio (unitless)	*EBR* (unitless)
Stump Spring	04-21-16 to 12-21-16	108.64	3.88	104.76	26.18	55.33	81.52	2.1	0.78
Hiko Springs	04-11-17 to 12-08-17	118.09	3.99	114.10	17.26	67.12	84.37	3.9	0.74
	03-30-18 to 12-04-18	121.93	3.22	118.71	16.97	69.56	86.53	4.1	0.73

Table 4. Actual evapotranspiration, precipitation, groundwater evapotranspiration, and uncertainties for each variable, Stump Spring and Hiko Springs, Clark County, southern Nevada, 2016–18.

[Units of measure are in millimeters per year. ***AET*:** Actual evapotranspiration. ***P*:** Precipitation. ***GWET*:** Groundwater evapotranspiration, computed using equation 5. **Symbol:** ±, plus or minus]

Site name	Analysis period	*AET* (measured)	*AET* (corrected)	*AET* uncertainty (±)	*P* (measured)	*P* (corrected)	*P* uncertainty (±)	*GWET* (computed)	*GWET* uncertainty (±)
Stump Spring	04-21-16 to 12-21-16	254	291	45	49	52	1	239	45
Hiko Springs	4-11-17 to 12-8-17	149	175	26	50	53	1	122	26
	3-30-18 to 12-4-18	150	178	29	77	81	2	97	29

Table 5. Cumulative normalized flux, Stump Spring and Hiko Springs, Clark County, southern Nevada, 2016–18.

[All numbers are in percent. **Cumulative normalized flux:** Turbulent-flux footprint from 25 to 300 meters (m) upwind of eddy-covariance sensors]

Site Name	Cumulative normalized flux					
	25 m	50 m	75 m	100 m	200 m	300 m
Stump Spring	34	61	73	80	90	94
Hiko Springs	81	92	95	97	98	99

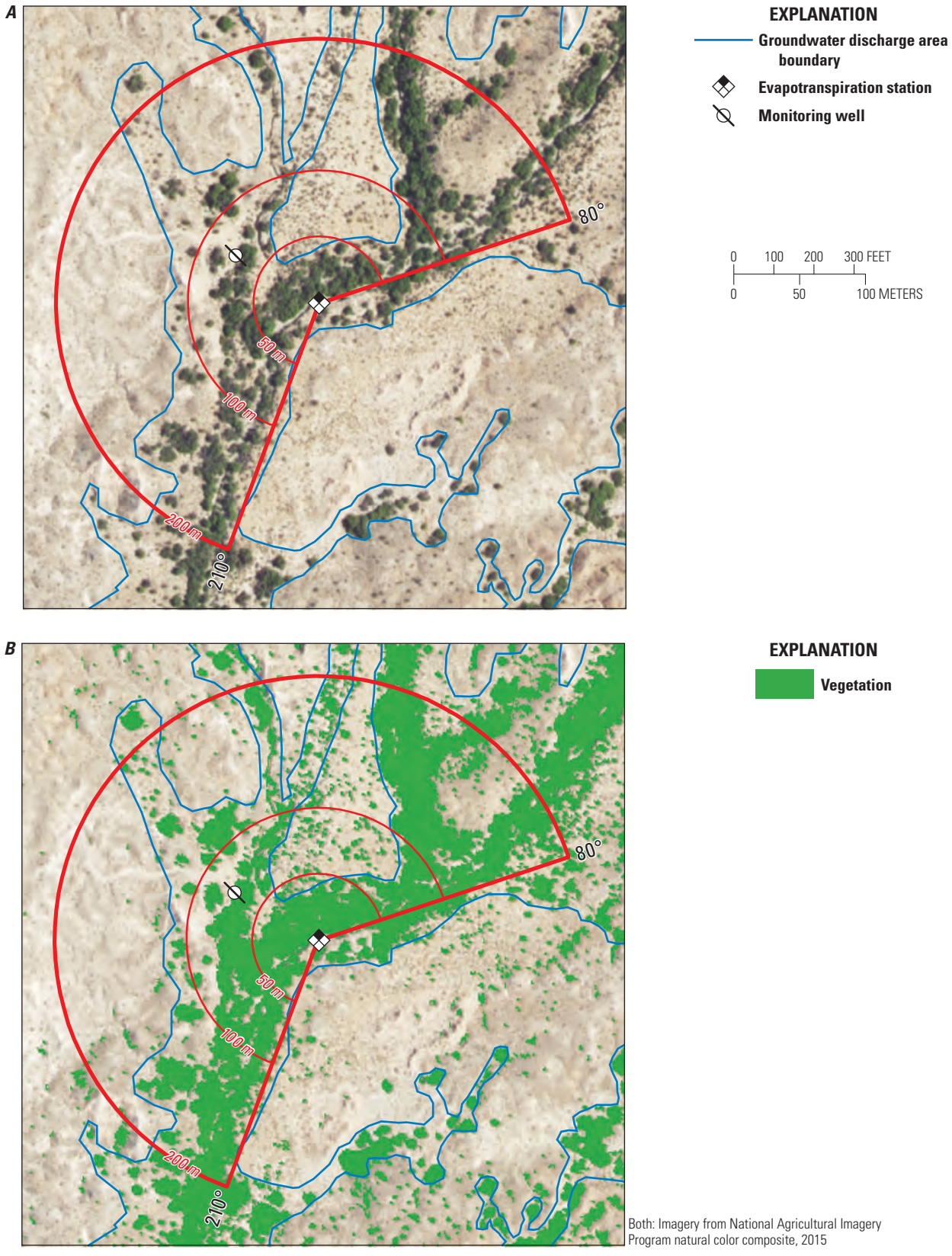

Figure 8. Eddy-covariance evapotranspiration station showing turbulent-flux source-area distances of 50, 100, and 200 meters over National Agriculture Imagery Program (NAIP) (*A*), vegetation classification based on NAIP (*B*), and scaled Normalized Difference Vegetation Index calculated from WorldView-2 (*C*), Stump Spring, Clark County, southern Nevada.

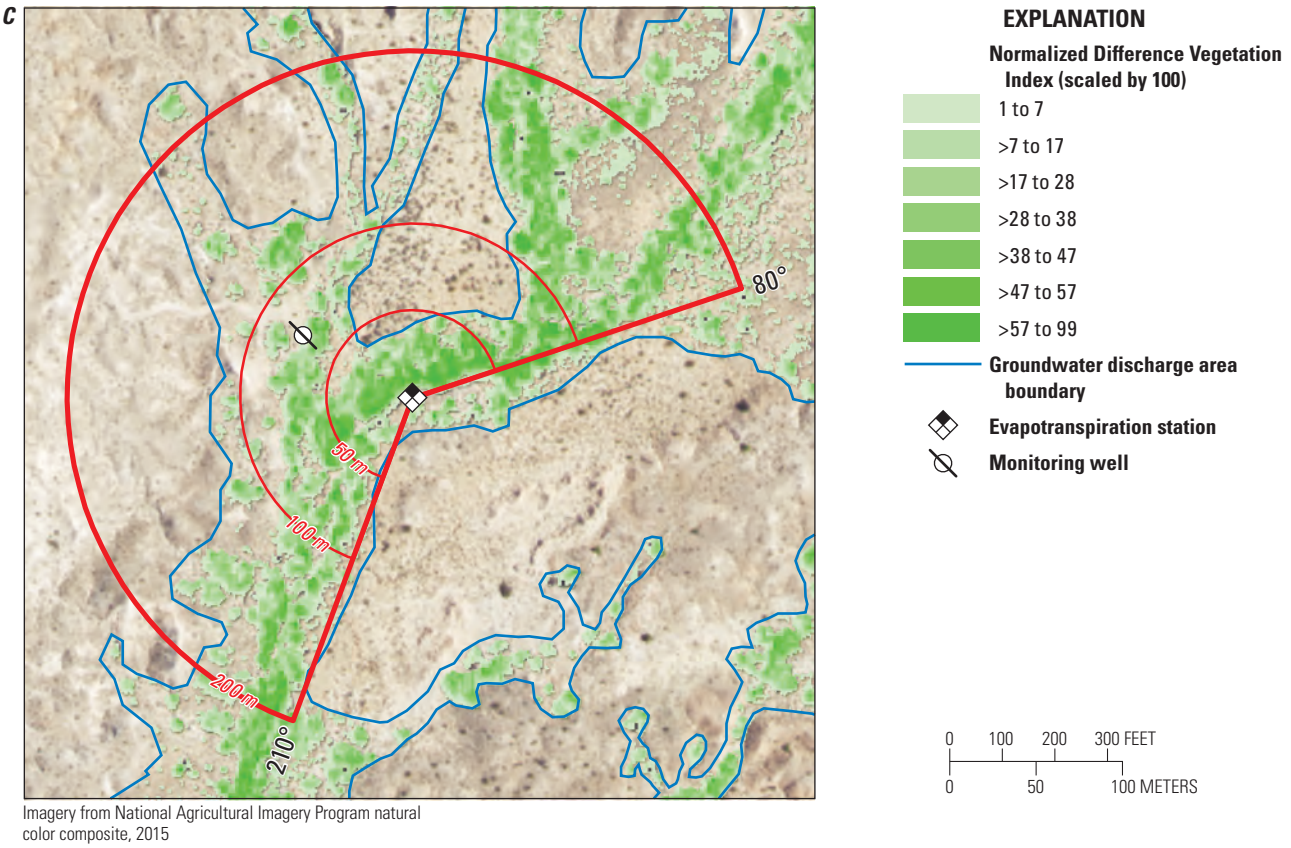

Imagery from National Agricultural Imagery Program natural color composite, 2015

Figure 8. —Continued

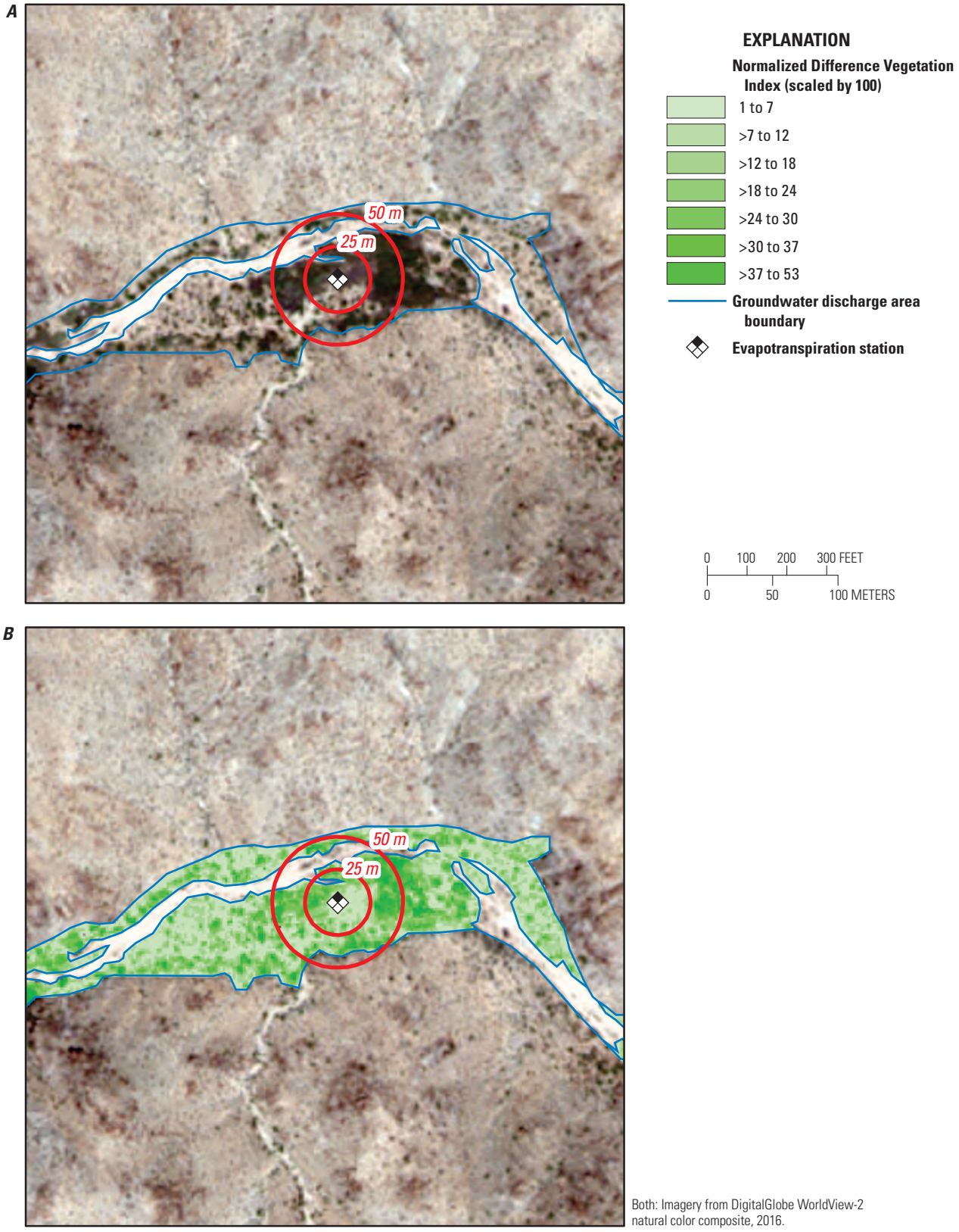

Figure 9. Eddy-covariance evapotranspiration station showing turbulent-flux source-area distances of 25 and 50 meters over WorldView-2 (*A*), and scaled Normalized Difference Vegetation Index calculated from WorldView-2 (*B*), Hiko Springs, Clark County, southern Nevada.

Table 6. Total area, phreatophyte vegetation area, phreatophyte cover, scaled Normalized Difference Vegetation Index (NDVI), site-scale phreatophyte cover, and site-scale footprint-weighted scaled NDVI estimates, Stump Spring, Clark County, southern Nevada, April 21–December 21, 2016.

[**Total area:** Total area at Stump Spring excludes wind azimuths from 80 to 210 degrees. **Abbreviations and symbol:** m, meter; m^2, square meter; –, Not applicable]

Site name	Turbulent-flux source-area distance (m)	Total area (m^2)	Phreatophyte vegetation area (m^2)	Phreatophyte cover (percent)	Mean scaled NDVI (dimensionless)
Stump Spring	0–50	6,620	4,436	67	28.6
	50–100	19,422	12,096	62	23.8
	100–200	71,880	32,306	45	20.6
	Total	97,921	48,838	–	–
	Site-scale (0-200 m) mean			50	–
	Site-scale (0-200 m) footprint-weighted mean			–	26.7

Table 7. Site-scale (0–50 meters) wind-direction-weighted scaled Normalized Difference Vegetation Index (NDVI) estimated as a function of wind direction and footprint-weighted scaled NDVI, Hiko Springs, Clark County, southern Nevada, April 11–December 8, 2017, and March 30–December 4, 2018.

[**Wind direction:** E, East; ENE, East-northeast; ESE, East-southeast; N, North; NE, Northeast; NNE, North-northeast; NW, Northwest; NNW, North-northwest; S, South; SE, Southeast; SSE, South-southeast; SSW, South-southwest; SW, Southwest; W, West; WNW, West-northwest; WSW, West-southwest. **Abbreviations and symbol:** n, Number of 30-minute measurements; m, meter; mm, millimeter; –, Not applicable]

Site name	Wind direction	Azimuth, in degrees		24 hours			Footprint-weighted mean NDVI (Dimensionless)	Daytime			Footprint-weighted and wind-proportional mean scaled NDVI (Dimensionless)
		Begin	End	n	Percent of total	*AET*, measured, (mm)		n	Percent of total	*AET*, measured (mm)	
Hiko Springs	ENE, E, ESE, SE	56.25	123.75	7,315	33	188	11.7	6,386	64	187	7.5
	SSE, S, SSW	123.75	213.75	2,708	12	43	7.5	1,694	17	42	1.3
	SW, WSW, W, WNW	213.75	303.75	12,019	54	39	22.6	1,766	18	32	4.0
	NW, NNW, N, NNE, NE	303.75	56.25	185	1	3	12.1	109	1	3	0.1
			Total	22,227	–	273	–	9,955	–	264	–
Site-scale footprint-weighted mean NDVI				–	–	–	13.5	–	–	–	–
Site-scale wind-direction-weighted mean NDVI				–	–	–	–	–	–	–	13.0

Groundwater Discharge Area Estimates

Delineated GDAs are shown figures 10 and 11. Based on NDVI values >0, the area of estimated phreatophytic vegetation was 59 ha within the Stump Spring GDA (the natural drainage), 49 ha for the Stump Spring ACEC GDA (defined by the ACEC boundary), and 7.2 ha within the Hiko Springs GDA (table 8). The areal distribution of phreatophytic vegetation was skewed toward lower NDVI values (figs. 12*A–C*). The area-weighted mean and maximum NDVI was 14.1/99 (Stump Spring GDA), 11.0/99 (Stump Spring ACEC GDA), and 13.4/53 (Hiko Springs GDA). The maximum NDVI at Stump Spring was roughly twice as great as at Hiko Springs.

The *GWET* rate applied in each GDA was derived using a linear relation between the computed *GWET* rates (table 4) and the site-scale NDVI estimates (tables 6 and 7). These linear relations assumed that *GWET* = 0 mm/yr at NDVI = 0, were fit to the site-scale computed *GWET* rate and NDVI for Stump Spring (*GWET* = 239 ±45 mm/yr, NDVI = 26.7) and Hiko Springs (*GWET* = 109 ±27 mm/yr, NDVI = 13.0), and were extrapolated to the maximum NDVI value in each GDA (fig. 13). Results indicate there was no significant difference between the slopes for these two areas. Furthermore, the similar *GWET*:NDVI ratios between the two sites provides confidence in the linearly extrapolated values.

The total *GWET* volume was computed by applying *GWET* rates estimated using the *GWET*–NDVI regression model to NDVI datasets in each GDA (table 8). The summed area of each NDVI value was multiplied by corresponding *GWET* rates (figs. 12*D–F*) and cumulative *GWET* was plotted as a function of NDVI (figs. 12*G–I*). Total *GWET* was computed by summing *GWET* estimated for each NDVI value in each GDA (table 8). At the Stump Spring GDA, for example, the area of phreatophytic vegetation is 59 ha and the *GWET* volume is 7.4 ±1.4 × 10^4 m^3/yr. Dividing the phreatophyte area by the GWET volume yields the area-weighted mean *GWET* rate of 126 mm/yr. Volume *GWET* uncertainties are based on *GWET* uncertainties given in table 4.

Comparison of Stump Spring Evapotranspiration Estimate with Published Estimates for Mesquite

The computed site-scale *GWET* rate for Stump Spring (table 4, fig. 13), and the maximum *GWET* rate predicted by the regression model (fig. 13), were compared with published *GWET* rates for mesquite. Groundwater evapotranspiration by mesquite has been measured for numerous studies using a variety of techniques. Published rates ranged from 128 to 975 mm/yr with canopy covers that ranged from 48 to 100 percent (table 9). A strong correlation (r^2 = 0.90) exists between published *GWET* rates and canopy cover (fig. 14). A point representing the *GWET* rate computed at Stump Spring (239 ±45 mm/yr) and estimated canopy cover (50 percent) was added to figure 14. A second point was added that assumes 100 percent canopy cover is represented by the maximum NDVI value for the Stump Spring GDA (99) with a predicted *GWET* rate from figure 13 (885 ±166 mm/yr). The error bars correspond to the estimated 19 percent GWET uncertainty (table 4). Without consideration for errors in the published data, which likely are similar to data in the current study, there is no significant difference between the slopes of these datasets since the slope of the published dataset is within the uncertainty of current study estimates. Furthermore, there is no significant difference between *GWET*-rate relations developed for Stump Spring and Hiko Springs (fig. 13). These similar slopes (figs. 13, 14) and overlapping uncertainties provide strong support for and increase confidence in the methodology and *GWET* estimates presented in this report.

Limitations of Methodology

The accuracy of *GWET* estimates presented in this report is limited primarily by assumptions inherent in eddy-covariance and upscaling methodologies, and the limited spatial extent and temporal period of *AET* and precipitation data collection. The eddy-covariance method represents the best available technology to measure *AET*. Site-scale *AET* estimates are considered to be of good quality because accepted data processing and correction methods were applied. Energy-balance ratios (Stump Spring = 0.78, Hiko Springs mean = 0.73) were similar to the average for previous studies. Site-scale *AET* estimates have an uncertainty of about 16 percent based on energy-balance deficiencies and gap-filling errors. This uncertainty estimate is considered reasonable and is consistent with previous studies in arid environments (Kampf and others, 2005, 15 percent; Garcia and others, 2015, 16 percent; Moreo and others, 2017, 15 percent).

Site-scale *GWET* estimates have an uncertainty of 19 percent at Stump Spring and 26 percent at Hiko Springs. Additional uncertainties resulting from upscaling *GWET* estimates using the *GWET*–NDVI regression model were not computed. Upscaling uncertainty typically is determined as the standard deviation between *GWET* estimates determined from multiple remotely sensed images. This method of determining upscaling uncertainty was not possible for the current study because only one image was available. Upscaling error was 4 percent based on 9 images in Dixie Valley (Garcia and others, 2015), and 1–8 percent based on 2 images for multiple basins in the Diamond Valley flow system (Berger and others, 2016; A. Garcia, U.S. Geological Survey, written commun., 2019).

The accuracy of *GWET* estimates presented in this report can be improved and uncertainty can be reduced with additional eddy-covariance and multi-spectral data, as some spatial and temporal variability in environmental and hydrologic conditions is expected. Establishing additional *AET* and precipitation measurement sites would help reduce the uncertainty in the relation between *GWET* rates and vegetation cover. Suitable measurement sites, however, are extremely limited in these small, ephemeral spring-discharge areas.

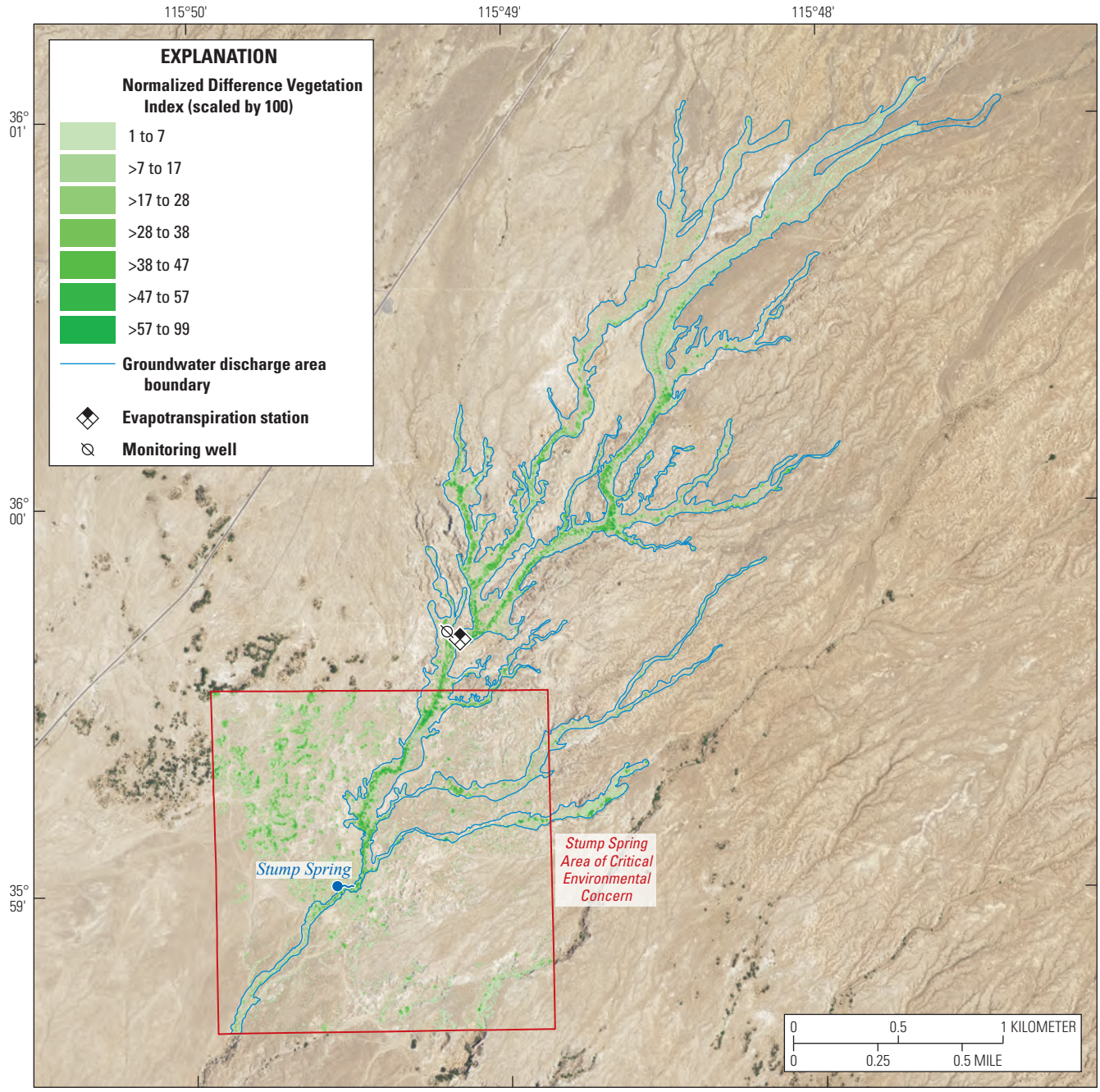

Base modified from U.S. Geological Survey and other Federal and State digital data, various scales. Imagery from National Agriculture Imagery Program natural color composite, 2015. Universal Transverse Mercator Projection, zone 11, World Geodetic System Datum of 1984

Figure 10. Delineated groundwater discharge area, Area of Critical Environmental Concern, and scaled Normalized Difference Vegetation Index distribution, Stump Spring, Clark County, southern Nevada.

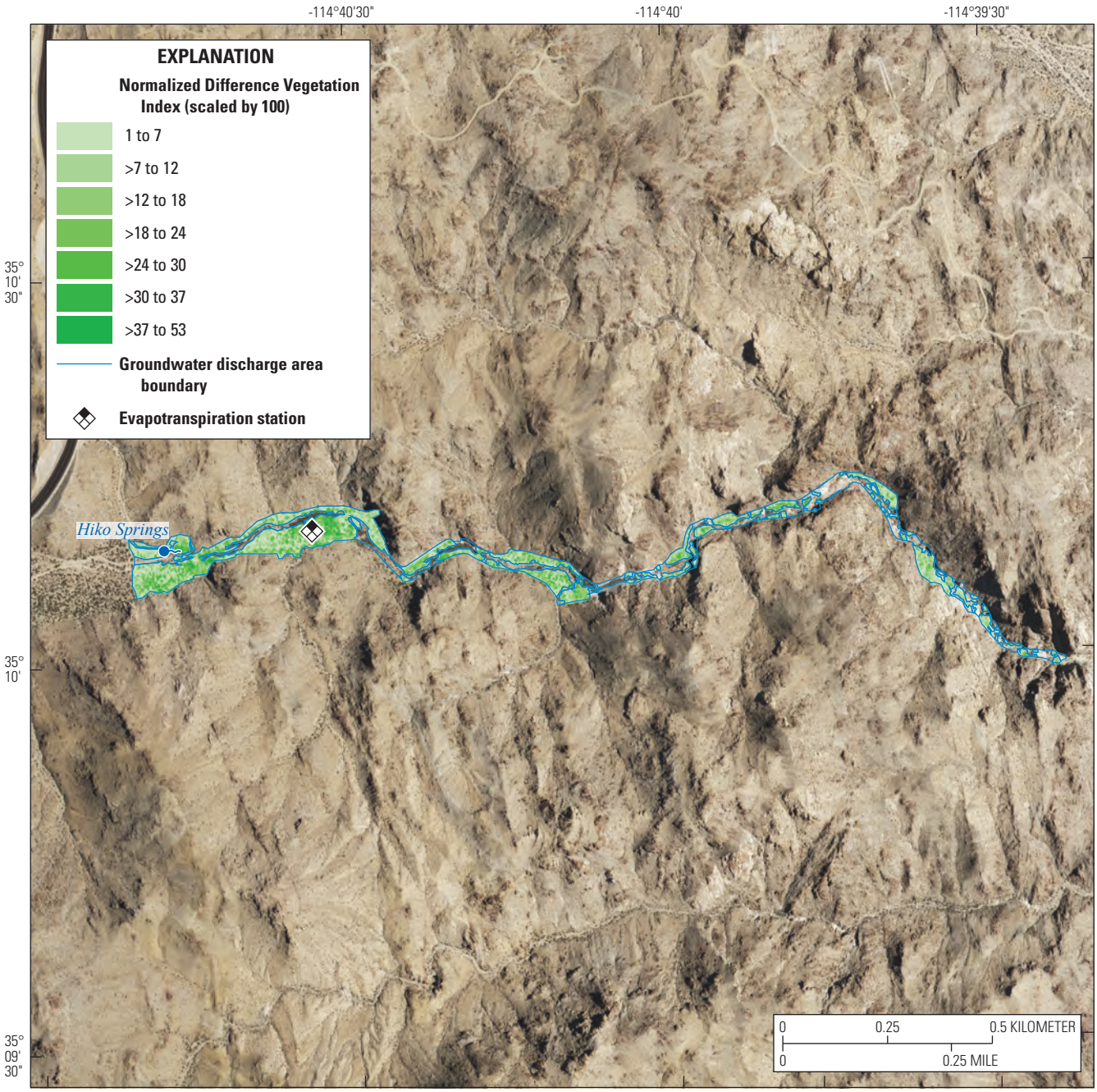

Base modified from U.S. Geological Survey and other Federal and State digital data, various scales. Imagery from National Agriculture Imagery Program natural color composite, 2015. Universal Transverse Mercator Projection, zone 11, World Geodetic System Datum of 1984

Figure 11. Delineated groundwater discharge area and scaled Normalized Difference Vegetation Index distribution, Hiko Springs, Clark County, southern Nevada.

Table 8. Phreatophytic vegetation areas, area-weighted mean groundwater evapotranspiration (GWET) rates, and *GWET* volumes and uncertainties, Stump Spring and Hiko Springs, Clark County, southern Nevada, 2016–18.

[**Groundwater discharge area:** ACEC, Area of Critical Environmental Concern. **Abbreviations:** *GWET*, Groundwater evapotranspiration; mm/yr, millimeters/year; m^3/yr, cubic meters per year]

Groundwater discharge area	Phreatophytic vegetation area (hectares)	Area-weighted mean *GWET* rate (mm/yr)	*GWET* volume (m^3/yr)	*GWET* uncertainty (m^3/yr)
Stump Spring	59	126	7.4×10^4	1.4×10^4
Stump Spring ACEC	49	98	4.9×10^4	0.9×10^4
Hiko Springs	7.2	112	0.8×10^4	0.2×10^4

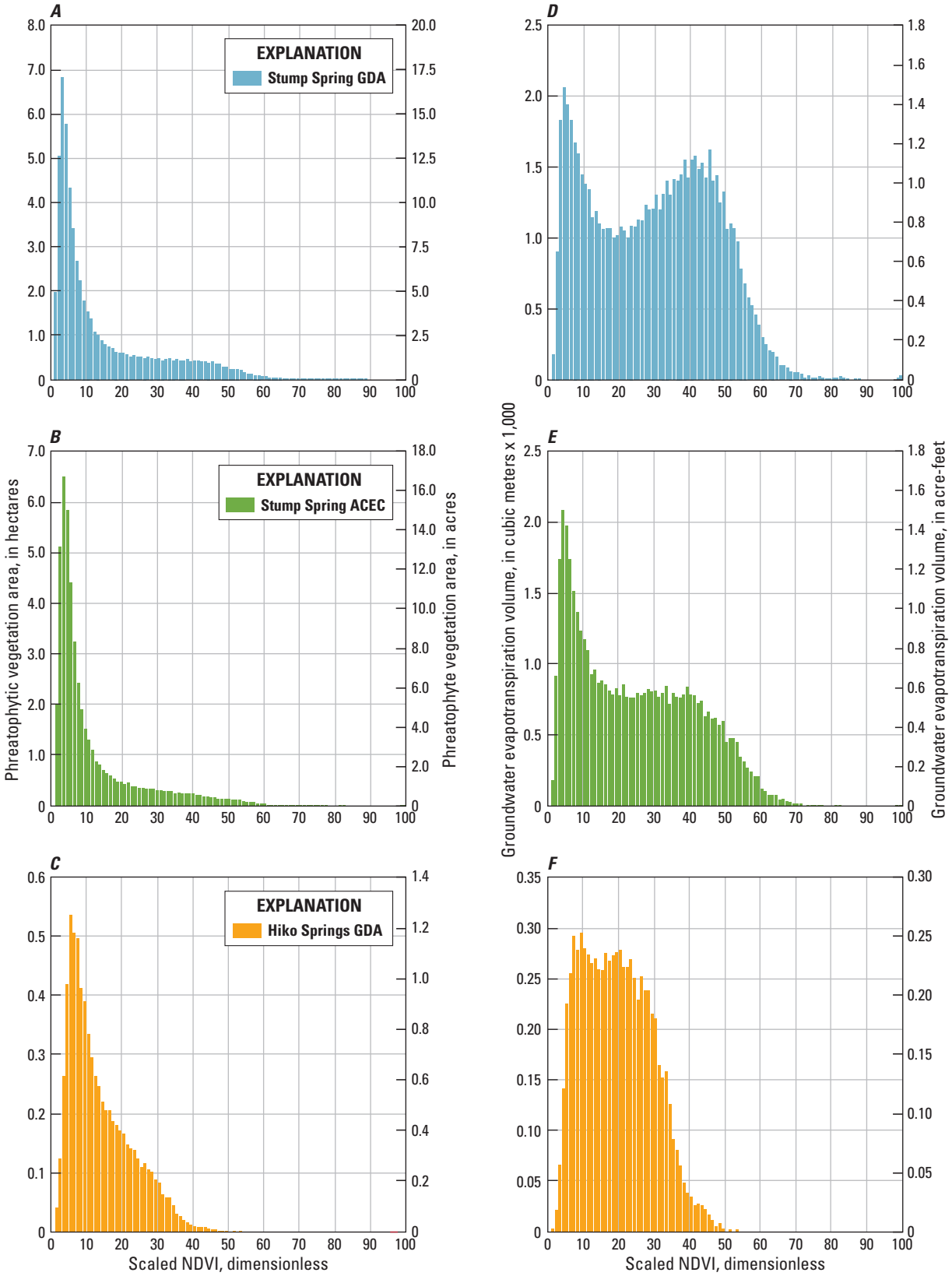

Figure 12. Phreatophytic vegetation areas (*A*–*C*), groundwater evapotranspiration volumes (*D*–*F*), and cumulative groundwater evapotranspiration volumes (*G*–*I*) estimated as a function of scaled Normalized Difference Vegetation Index (NDVI), Stump Spring and Hiko Springs, Clark County, southern Nevada. ACEC, Area of Critical Environmental Concern; GDA, groundwater discharge area.

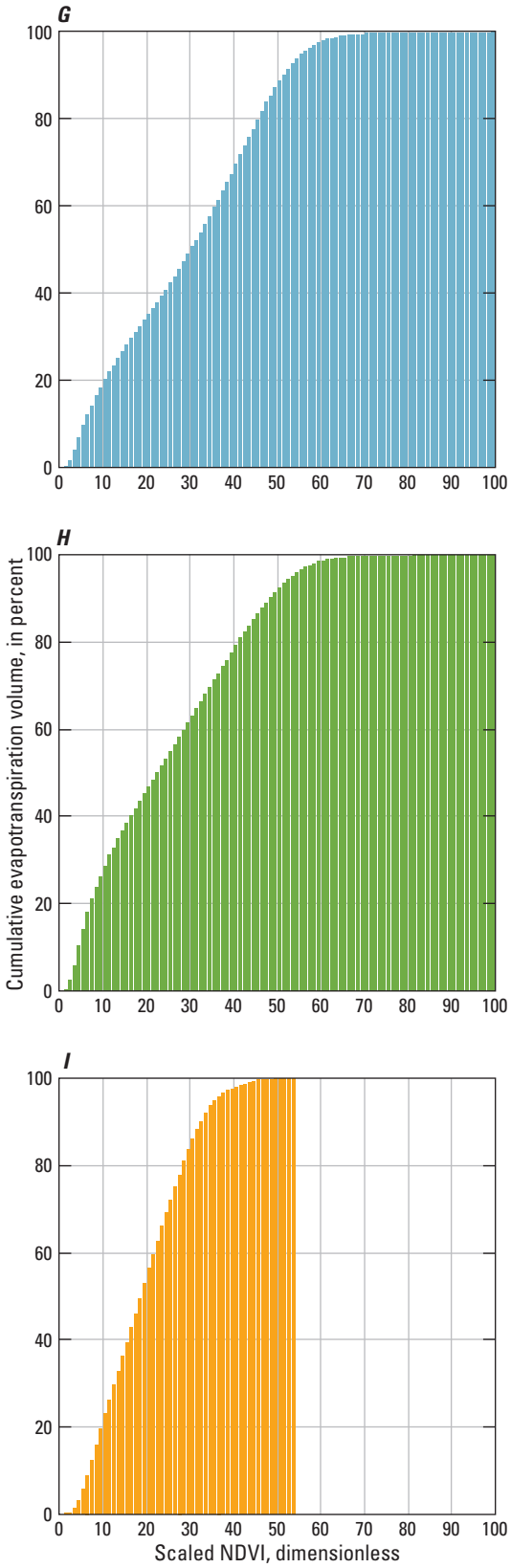

Figure 12. —Continued

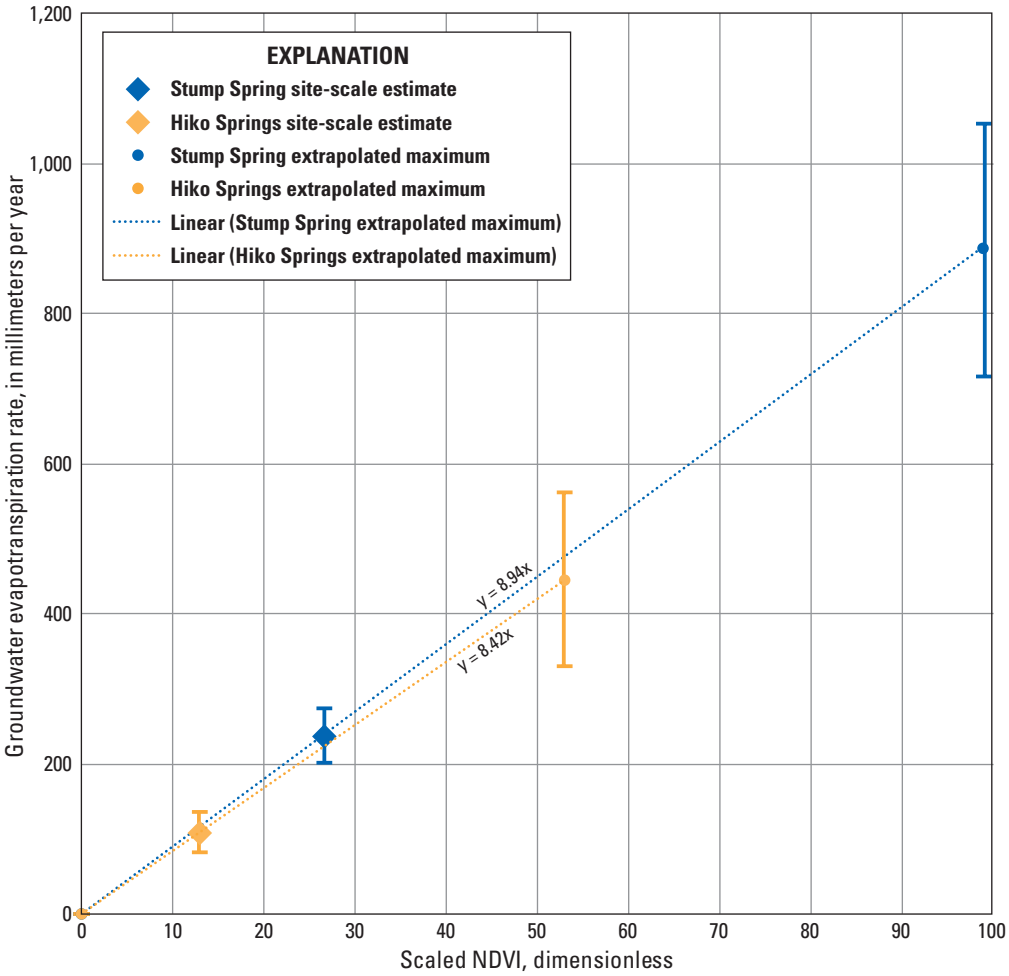

Figure 13. Groundwater evapotranspiration rates determined as a function of computed site-scale groundwater evapotranspiration and Normalized Difference Vegetation Index (NDVI) estimates, and uncertainty (error bars), Stump Spring and Hiko Springs, Clark County, southern Nevada.

Table 9. Published groundwater evapotranspiration rates and canopy covers for mesquite.

[**Location:** AZ, Arizona; CA, California; NV, Nevada. **Measurement method:** BREB, Bowen-ratio energy budget; EC, eddy covariance; N/A, not applicable. ***GWET*:** Groundwater evapotranspiration. **Abbreviation and symbol:** mm/yr, millimeters per year; –, No remark]

Citation	Study period	Location	Vegetation type	Measurement method	Canopy Cover (percent)	*GWET* (mm/yr)	Remarks
Gatewood and others (1950)	1943–44	Gila River, Safford, AZ	Mesquite woodland	Transpiration well	100	826	Groundwater use determined by multiplying daily water table decline by specific yield
Bureau of Reclamation (1995)	1995	Lower Colorado River Basin, CA	Honey and screwbean mesquite	BREB	65	427	Average of 50–80 percent reported canopy cover
Scott and others (2000)	1997–98	San Pedro River, Lewis Springs, AZ	Mesquite shrubland	BREB	50	128	–
Leenhouts and others (2005)	2001–03	San Pedro Basin, AZ	Velvet mesquite	EC	75	464	–
DeMeo and others (2008)	2003–06	Muddy River, NV	Mesquite	BREB	100	975	–
Scott and others (2008)	2003–05	San Pedro River, Lewis Springs, AZ	Mesquite woodland	EC	75	490	–
Scott and others (2014)	2003–07	San Pedro River, AZ	Mesquite woodland	EC	70	449	–
Meader (2015)	1943–44	Gila River, Safford, AZ	Mesquite woodland	N/A	48	318	Re-evaluation of Gatewood and others (1950)

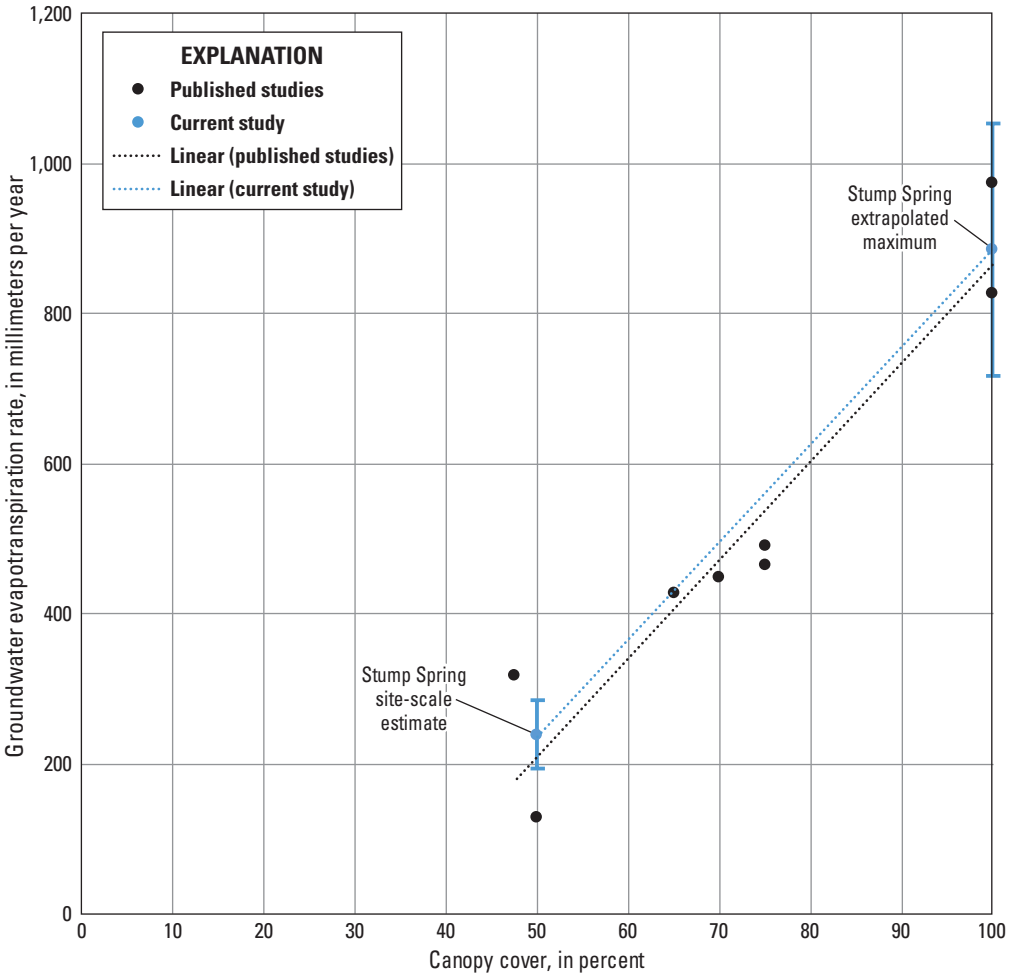

Figure 14. Published groundwater evapotranspiration rates and canopy covers for mesquite, and current study groundwater evapotranspiration rates with uncertainty (error bars) and canopy cover from Stump Spring, Clark County, southern Nevada.

Summary and Conclusions

In cooperation with the Bureau of Land Management, the U.S. Geological Survey conducted a study to estimate annual groundwater discharge by evapotranspiration (*GWET*) from the phreatophytic vegetation at Stump Spring and Hiko Springs. These desert riparian areas in the southern Nevada are characterized by ephemeral springs in lowland washes. The phreatophytes at Stump Spring consisted primarily of western honey mesquite [*Prosopis glandulosa* var. *torreyana* (L.D. Benson) M.C. Johnst.], a deciduous, thorny tree with a mean height of about 4 meters (m). The phreatophytes at Hiko Springs consisted primarily of mixed shrubs with a mean height of about 1 m.

Groundwater discharge by evapotranspiration was estimated by developing relations between site-scale computed *GWET* rates and Normalized Difference Vegetation Index (NDVI) datasets representative of the phreatophytic vegetation in each groundwater discharge area (GDA). Site-scale *GWET* was computed by subtracting measured precipitation from actual evapotranspiration (AET). An instrumented station established at each study location was equipped with eddy-covariance and other sensors necessary to continuously measure 30-minute AET and major energy-balance fluxes. Precipitation was measured with a National Weather Service-style non-recording precipitation gage. A representative site-scale NDVI value was computed based on turbulent-flux source-area estimates and wind-direction data. Site-scale *GWET* was scaled up to each GDA using relations developed with site-scale NDVI. Groundwater discharge areas were mapped by visual interpretation of 2015 1-m resolution National Agriculture Imagery Program (NAIP) aerial imagery, and the phreatophytes within each GDA were characterized using NDVI datasets. The NDVI is a dimensionless vegetation index that indicates the relative abundance, health, and vigor of green vegetation. The NDVI was calculated from 1.84-m resolution WorldView 2 (WV2) imagery and rescaled to 1–99.

Site-scale results are as follows:

1. Stump Spring 2016—
   a. Energy-balance ratio = 0.78,
   b. Corrected AET = 291 ±45 millimeters (mm),
   c. Corrected precipitation = 52 ±1 mm,
   d. *GWET* T = 239 ±45 mm, and
   e. Footprint-weighted-mean scaled NDVI = 26.7.
2. Hiko Springs 2017—
   a. Energy-balance ratio = 0.74,
   b. Energy-balance corrected AET = 175 ±26 mm,
   c. Corrected precipitation = 53 ±1 mm,
   d. *GWET* = 122 ±26 mm, and
   e. Footprint- and daytime-wind-weighted-mean scaled NDVI = 13.0.
3. Hiko Springs 2018—
   a. Energy-balance ratio = 0.73,
   b. Energy-balance corrected AET = 178 ±29 mm,
   c. Corrected precipitation = 81 ±2 mm, and
   d. *GWET* = 97 ±29 mm.

Groundwater discharge area estimates are as follows:

1. Stump Spring GDA—
   a. Phreatophyte area = 59 hectares (ha) (145 acres),
   b. Area-weighted mean *GWET* rate = 126 mm/year (yr) [0.41 feet (ft)/yr],
   c. *GWET* = 7.4×10^4 cubic meters (m^3/yr) (60 acre-ft/yr), and
   d. *GWET* uncertainty = 1.4×10^4 m^3/yr (11 acre-ft/yr).
2. Stump Spring Area of Critical Environmental Concern (ACEC)—
   a. Phreatophyte area = 49 ha [122 acres],
   b. Area-weighted mean *GWET* rate = 98 mm/yr (0.32 ft/yr),
   c. *GWET* = 4.9×10^4 m^3/yr (39 acre-ft/yr), and
   d. *GWET* uncertainty = 0.9×10^4 m^3/yr (7 acre-ft/yr).
3. Hiko Springs GDA—
   a. Phreatophyte area = 7.2 ha (18 acres),
   b. Area-weighted mean *GWET* rate = 112 mm/yr (0.37 ft/yr),
   c. *GWET* = 0.8×10^4 m^3/yr (6.6 acre-ft/yr), and
   d. *GWET* uncertainty = 0.2×10^4 m^3/yr (1.6 acre-ft/yr).

Groundwater follows an intermediate flow path from recharge areas in the Spring Mountains to the Stump Spring discharge area, meaning groundwater inflow is relatively constant from year to year. Evidence for this is shown by the stable groundwater levels reported for Stump Spring well. Annual minimum depth-to-groundwater levels declined from 7.89 to 8.21 m below land surface from 2010 to 2018, indicating an interannual variability rate of just 0.04 m/yr. As such, *GWET* also is expected to be relatively constant from year to year; therefore, the *GWET* estimates presented in this report are considered representative of the long-term mean within the limits of stated uncertainties.

Hiko Springs likely receives all groundwater inflow from focused recharge of local, episodic precipitation events. Floodwaters collect upgradient, then move eastward funneling through the canyon toward the Colorado River. Because this recharge mechanism can be highly variable from year to year, an unplanned second year of data were collected (2018) to evaluate interannual *GWET* variability. Even though measured precipitation increased at the Hiko site from 2017 to 2018

(table 4), there was no indication that any substantial flooding occurred in this drainage after the September 2015 event. Consequently, with limited recharge and continued *GWET* during the 2017 growing season, an increase in water-table depth and corresponding decrease in the *GWET* rate was expected in 2018 compared to 2017. Although no water-level data are available for the Hiko Springs drainage to confirm an increase in the water table, the *GWET* rate decreased by 21 percent in 2018 compared to 2017. In addition to variability in annual *GWET* rates, the area of phreatophytic vegetation also can vary annually as shown by the September 2015 flood, which resulted in a 14-percent decrease in vegetation. Although the consistency of annual recharge is sufficient to maintain a small population of phreatophytes—apparently owing to the relatively large upgradient contributing area and adequate groundwater storage capacity—based on the preceding evidence, it cannot be stated with confidence that estimates presented in this report for Hiko Springs are indicative of the long-term mean in this highly dynamic environment.

Acknowledgments

The authors wish to thank the Bureau of Land Management Las Vegas Field Office for supporting this research effort, including District Hydrologist Boris Poff for his knowledge and leadership and District Botanist Lara Kobelt for conducting the plant survey at Hiko Springs.

References Cited

Baldocchi, D.D., 2003, Assessing the eddy covariance technique for evaluating carbon dioxide exchange rates of ecosystems—Past, present, and future: Global Change Biology, v. 9, no. 4, p. 479–492.

Berger, D.L., Mayers, C.J., Garcia, C.A., Buto, S.G., and Huntington, J.M., 2016, Budgets and chemical characterization of groundwater for the Diamond Valley flow system, central Nevada, 2011–12: U.S. Geological Survey Scientific Investigations Report 2016–5055, 83 p., https://doi.org/10.3133/sir20165055.

Brutsaert, W.H., 1982, Evaporation into the atmosphere: Boston, D. Reidel Publishing, 299 p., https://doi.org/10.1007/978-94-017-1497-6.

Bureau of Reclamation, 1995, Vegetation management study, lower Colorado River, phase II: Bureau of Reclamation, Boulder City, Nevada,, 72 p.

Buto, S.G., 2020, Geospatial data to support estimates of annual groundwater discharge by evapotranspiration from areas of spring-fed riparian vegetation, Stump Spring and Hiko Springs, Clark County, southern Nevada: U.S. Geological Survey data release, https://doi.org/10.5066/P9BG3VKP.

Campbell, G.S., and Norman, J.M., 1998, An introduction to environmental biophysics (2d ed.).: New York, Springer-Verlag, 286 p.

Campbell Scientific, Inc., 2010b, Instruction manual for CSAT3 three dimensional sonic anemometer, revision 6/10: Logan, Utah, Campbell Scientific, Inc., accessed September 28, 2011, at http://s.campbellsci.com/documents/us/manuals/csat3.pdf.

Campbell Scientific, Inc., 2010a, Instruction manual for KH2O krypton hygrometer, revision 2/10: Logan, Utah, Campbell Scientific, Inc., accessed December 23, 2010, at http://s.campbellsci.com/documents/us/manuals/kh20.pdf.

Campbell Scientific, Inc., 2012, Instruction manual for HFP01 soil heat flux plate, revision 7/12: Logan, Utah, Campbell Scientific, Inc., accessed May 1, 2014, at http://s.campbellsci.com/documents/us/manuals/hfp01.pdf.

Campbell Scientific, Inc., 2016, Instruction manual for CS616 and CS625 water content reflectometers, revision February 2016: Logan, Utah, Campbell Scientific, Inc., accessed March 11, 2020, at https://s.campbellsci.com/documents/af/manuals/cs616.pdf.

Clement, R., 2012, EdiRe data software, version 1.5.0.32: Edinburgh, Scotland, University of Edinburgh, accessed 2012, at https://www.geos.ed.ac.uk/homes/jbm/micromet/EdiRe/.

DeMeo, G.A., Laczniak, R.J., Boyd, R.A., Smith, J.L., and Nylund, W.E., 2003, Estimated ground-water discharge by evapotranspiration from Death Valley, California, 1997–2001: U.S. Geological Survey Water-Resources Investigations Report 03–4254, 27 p., https://pubs.usgs.gov/wri/wrir034254/.

DeMeo, G.A., Smith, J.L., Damar, N.A., and Darnell, J., 2008, Quantifying ground-water and surface-water discharge from evapotranspiration processes in 12 hydrographic areas of the Colorado Regional Ground-Water Flow System, Nevada, Utah, and Arizona: U.S. Geological Survey Scientific Investigations Report 2008–5116, 22 p., https://pubs.usgs.gov/sir/2008/5116/.

DigitalGlobe, 2010, The benefits of the eight spectral bands of WorldView-2: Digital Globe whitepaper, 12 p., accessed May 18, 2019, at https://dg-cms-uploads-production.s3.amazonaws.com/uploads/document/file/35/DG-8SPECTRAL-WP_0.pdf.

Doherty, J., 2010b, Addendum to the PEST manual: Brisbane, Australia, Watermark Numerical Computing.

Doherty, J., 2010a, PEST, Model-independent parameter estimation—User manual (5th ed., with slight additions): Brisbane, Australia, Watermark Numerical Computing.

Fenelon, J.M., Halford, K.J., and Moreo, M.T., 2016, Delineation of the Pahute Mesa–Oasis Valley groundwater basin, Nevada (ver. 1.1, May 2016): U.S. Geological Survey Scientific Investigations Report 2015–5175, 40 p., https://doi.org/10.3133/sir20155175.

Fenelon, J.M., and Moreo, M.T., 2002, Trend analysis of ground-water levels and spring discharge in the Yucca Mountain Region, Nevada and California, 1960–2000: U.S. Geological Survey Water-Resources Investigations Report 2002–4178, 97 p., https://pubs.usgs.gov/wri/wrir024178/.

Ffolliott, P.F., Baker, M.B., DeBano, L.F., and Neary, D.G., 2004, Introduction, chap. 1 *of* Baker, M.B., and others, eds., Riparian areas of the southwestern United States—Hydrology, ecology, and management: Boca Raton, Florida, CRC press, p. 1–9.

Foken, T., 2008, Micrometeorology: Berlin and Heidelberg, Germany, Springer-Verlag, 306 p.

Foken, T., Leuning, R., Oncley, S., Mauder, M., and Aubinet, M., 2012, Corrections and data quality control, chap. 4 *of* Aubinet, M., Vesala, T., and Papale, D., eds., Eddy covariance—A practical field guide to measurement and data analysis: Dordrecht, The Netherlands, Heidelberg, Germany, London, and New York, Springer, p. 85–131.

Freeze, R.A., and Cherry, J.A., 1979, Groundwater: Englewood Cliffs, New Jersey, Prentice-Hall, 604 p.

Garcia, C.A., Huntington, J.M., Buto, S.G., Moreo, M.T., Smith, J.L., and Andraski, B.J., 2015, Groundwater discharge by evapotranspiration, Dixie Valley, west-central Nevada, March 2009–September 2011: U.S. Geological Survey Professional Paper 1805, 90 p., https://doi.org/10.3133/pp1805.

Gatewood, J.S., Robinson, T.W., Colby, B.R., Hem, J.D., and Halpenny, L.C., 1950, Use of water by bottom-land vegetation in lower Safford Valley, Arizona: U.S. Geological Survey Water Supply Paper 1103, 210 p., https://pubs.er.usgs.gov/publication/wsp1103.

Halford, K., Garcia, C.A., Fenelon, J., and Mirus, B., 2012, Advanced methods for modeling water-levels and estimating drawdowns with SeriesSEE, an Excel add-in: U.S. Geological Survey Techniques and Methods, book 4, chap. F4, 28 p., accessed October 2014, at https://pubs.usgs.gov/tm/tm4-F4/.

Harrill, J.R., 1986, Ground-water storage depletion in Pahrump Valley, Nevada-California, 1962–1975: U.S. Geological Survey Water-Supply Paper 2279, 53 p., https://pubs.er.usgs.gov/publication/wsp2279.

Heaton, J.S., Miao, X., Von Seckendorff Hoff, K., Charlet, D., Cashman, P., Trexler, J., Grimmer, A., and Patil, R., 2011, Ecosystem indicators final report 2005-UNR-578: Reno, University of Nevada, Report to Clark County MSHCP, 36 p., http://www.clarkcountynv.gov/airquality/dcp/Documents/Library/dcp%20reports/2011/Geomorphology%20and%20Vegetation%20Mapping%20UNR%20578%20Jun%202011.pdf.

Højstrup, J., 1993, A statistical data screening procedure: Measurement Science & Technology, v. 4, no. 2, p. 153–157.

Houghton, J.G., Sakamato, C.M., and Gifford, R.O., 1975, Nevada's weather and climate: Nevada Bureau of Mines and Geology Special Publication 2, 78 p.

Jensen, J.R., 2000, Remote sensing of the environment—An earth resource perspective: Upper Saddle River, New Jersey, Prentice Hall, 544 p.

Kaimal, J.C., and Finnigan, J.J., 1994, Atmospheric boundary layer flows—Their structure and measurement: New York, Oxford University Press, 289 p.

Kampf, S.K., Tyler, S.W., Ortiz, C.A., Munoz, J.F., and Adkins, P.L., 2005, Evaporation and land surface energy budget at the Salar de Atacama, northern Chile: Journal of Hydrology (Amsterdam), v. 310, nos. 1–4, p. 236–252.

Knochenmus, L.A., Laczniak, R.J., Moreo, M.T., and others, 2008, Ground-water conditions, *in* Welch, A.H., Bright, D.J., and Knochenmus, L.A., eds., Water resources of the Basin and Range carbonate-rock aquifer system, White Pine County, Nevada, and adjacent areas in Nevada and Utah: U.S. Geological Survey Scientific Investigations Report 2007–5261, p. 37–42, https://pubs.usgs.gov/sir/2007/5261/.

Kormann, R., and Meixner, F., 2001, An analytical footprint model for non-neutral stratification: Boundary-Layer Meteorology, v. 99, no. 2, p. 207–224, https://doi.org/10.1023/A:1018991015119.

Laczniak, R.J., DeMeo, G.A., Reiner, S.R., Smith, J.L., and Nylund, W.E., 1999, Estimates of ground-water discharge as determined from measurements of evapotranspiration, Ash Meadows area, Nye County, Nevada: U.S. Geological Survey Water-Resources Investigations Report 99–4079, 70 p., http://pubs.er.usgs.gov/publication/wri994079.

Laczniak, R.J., Flint, A.L., Moreo, M.T., and others, 2008, Ground-water budgets, *in* Welch, A.H., Bright, D.J., and Knochenmus, L.A., eds., Water resources of the Basin and Range carbonate-rock aquifer system, White Pine County, Nevada, and adjacent areas in Nevada and Utah: U.S. Geological Survey Scientific Investigations Report 2007–5261, p. 43–82., http://pubs.er.usgs.gov/publication/sir20075261.

Laczniak, R.J., Smith, J.L., and DeMeo, G.A., 2006, Annual ground-water discharge by evapotranspiration from areas of spring-fed riparian vegetation along the eastern margin of Death Valley, 2000–02: U.S. Geological Survey Scientific Investigations Report 2006–5145, 36 p., http://pubs.er.usgs.gov/publication/sir20065145.

Laczniak, R.J., Smith, J.L., Elliott, P.E., DeMeo, G.A., Chatigny, M.A., and Roemer, G.J., 2001, Ground-water discharge determined from estimates of evapotranspiration, Death Valley regional flow system, Nevada and California: U.S. Geological Survey Water-Resources Investigations Report 2001–4195, 51 p., http://pubs.er.usgs.gov/publication/wri014195.

Law, B.E., Loescher, H.W., Boden, T.A., Hargrove, W.W., and Hoffman, F.M., 2005, AmeriFlux site evaluation and recommendations for network enhancement: Oak Ridge National Laboratory, 27 p., accessed May 5, 2014, at http://citeseerx.ist.psu.edu/viewdoc/download?doi=10.1.1.187.5356&rep=rep1&type=pdf.

Lee, T.M., and Swancar, A., 1997, Influence of evaporation, ground water, and uncertainty in the hydrologic budget of Lake Lucerne, a seepage lake in Polk County, Florida: U.S. Geological Survey Water-Supply Paper 2439, 61 p., https://fl.water.usgs.gov/publications/Abstracts/wsp2439_lee.html.

Leenhouts, J.M., Stromberg, J.C., and Scott, R.L., 2005, Hydrologic requirements of and consumptive groundwater use by riparian vegetation along the San Pedro River, Arizona: U.S. Geological Survey Scientific Investigations Report 2005–5163, 154 p., https://pubs.usgs.gov/sir/2005/5163/.

Leuning, R., van Gorsel, E., Massman, W.J., and Isaac, P.R., 2012, Reflections on the surface energy imbalance problem: Agricultural and Forest Meteorology, v. 156, p. 65–74.

Longwell, C.R., Pampeyan, E.H., Bowyer, B., and Roberts, R.J., 1965, Geology and mineral deposits of Clark County, Nevada, 1:250,000: Nevada Bureau of Mines and Geology, Bulletin 62, https://pubs.nbmg.unr.edu/Geol-mineral-of-Clark-Co-p/b062.htm.

Malmberg, G.T., 1967, Hydrology of the valley-fill and carbonate-rock reservoirs, Pahrump Valley, Nevada-California: U.S. Geological Survey Water-Supply Paper 1832, 47 p., https://pubs.er.usgs.gov/publication/wsp1832.

Maxey, G.B., and Jameson, C.H., 1948, Geology and water resources of Las Vegas, Pahrump, and Indian Spring Valleys, Clark and Nye Counties, Nevada: Nevada State Engineer, Water Resources Bulletin 5, 121 p.

Meader, N., 2015, A review of riparian mesquite and crop water use: Cascabel Conservation Association, 48 p., accessed March 14, 2019, at http://cascabelconservation.org/downloads/Alfalfa-Mesquite%20Full%20Report-02-19-15.pdf.

Meinzer, O.E., 1927, Plants as indicators of ground water: U.S. Geological Survey Water-Supply Paper 577, 95 p., http://pubs.er.usgs.gov/publication/wsp577.

Moore, C.J., 1986, Frequency response corrections for eddy correlation systems: Boundary-Layer Meteorology, v. 37, p. 17–35.

Moreo, M.T., Andraski, B.J., and Garcia, C.A., 2017, Groundwater discharge by evapotranspiration, flow of water in unsaturated soil, and stable isotope water sourcing in areas of sparse vegetation, Amargosa Desert, Nye County, Nevada: U.S. Geological Survey Scientific Investigations Report 2017–5079, 55 p., https://doi.org/10.3133/sir20175079.

Moreo, M.T., Andraski, B.J., Orozco, E.L., and Kauble, R.K., 2018, Selected evapotranspiration data, Amargosa Desert Research Site, Nye County, Nevada, 7/5/2011–1/1/2017: U.S. Geological Survey data release, https://doi.org/10.5066/F7ZS2VQR.

Moreo, M.T., Laczniak, R.J., and Stannard, D.I., 2007, Evapotranspiration rate estimates of vegetation typical of ground-water discharge areas in the Basin and Range carbonate-rock aquifer system, Nevada and Utah, September 2005–August 2006: U.S. Geological Survey Scientific Investigations Report 2007–5078, 36 p., https://pubs.er.usgs.gov/publication/sir20075078.

Moreo, M.T., Senay, G.B., Flint, A.L., Damar, N.A., Laczniak, R.J., and Hurja, J., 2014, Hydroclimate of the Spring Mountains and Sheep Range, Clark County, Nevada: U.S. Geological Survey Scientific Investigations Report 2014–5142, 38 p., https://doi.org/10.3133/sir20145142.

Moreo, M.T., and Swancar, A., 2013, Evaporation from Lake Mead, Nevada and Arizona, March 2010 through February 2012: U.S. Geological Survey Scientific Investigations Report 2013–5229, 40 p., https://doi.org/10.3133/sir20135229.

National Weather Service, 2018, The climate of Las Vegas, Nevada: Publication of National Weather Service, Las Vegas, Nevada, 153 p., accessed 2020, at https://www.wrh.noaa.gov/vef/climate/LasVegasClimateBook/index.php.

Nevada Office of the State Engineer, 2007, Ruling #5750: Nevada Division of Water Resources, 22 p., http://images.water.nv.gov/images/rulings/5750r.pdf.

Pavelko, M.T., 2014, Site-characteristic and hydrologic data for selected wells and springs on Federal land in Clark County, Nevada: U.S. Geological Survey Data Series 864, 18 p., https://doi.org/10.3133/ds864.

Quiring, R.F., 1965, Annual precipitation amount as a function of elevation in Nevada south of 38 1/2 degrees latitude: Las Vegas, Nevada, U.S. Weather Bureau Research Station, 14 p.

Rannik, U., Sogachev, A., Foken, T., Gockede, M., Kljun, N., Leclerc, M., and Vesala, T., 2012, Footprint analysis chap. 8 *of* Aubinet, M., Vesala, T., Papale, D., eds., Eddy covariance—A practical field guide to measurement and data analysis: Dordrecht, The Netherlands, Heidelberg, Germany, London, and New York, Springer, p. 211–261.

Reiner, S.R., Laczniak, R.J., DeMeo, G.A., Smith, J.L., Elliott, P.E., Nylund, W.E., and Fridrich, C.J., 2002, Ground-water discharge determined from measurements of evapotranspiration, other available hydrologic components, and shallow water-level changes, Oasis Valley, Nye County, Nevada: U.S. Geological Survey Water-Resources Investigations Report 01–4239, 65 p., https://pubs.usgs.gov/wri/wri014239/.

Richards, J.A., and Jia, X., 1999, Remote sensing and digital image analysis: Berlin, Springer-Verlag, 240 p.

Rouse, J.W., Haas, R.H., Schell, J.A., and Deering, D.W., 1974, Monitoring vegetation systems in the Great Plains with ERTS, *in* Proceedings of the Third Earth Resources Technology Satellite-1 Symposium, Washington, D.C., December 10–14, 1973: National Aeronautics and Space Administration, Scientific and Technical Information Office, p. 309–317.

Schotanus, P., Nieuwstadt, F.T.M., and de Bruin, H.A.R., 1983, Temperature measurement with a sonic anemometer and its application to heat and moisture fluxes: Boundary-Layer Meteorology, v. 26, p. 81–93.

Schuepp, P.H., LeClerc, M.Y., Macpherson, J.I., and Desjardins, R.L., 1990, Footprint prediction of scalar fluxes from analytical solutions of the diffusion equation: Boundary-Layer Meteorology, v. 50, p. 355–373.

Scott, R.L., Cable, W.L., Huxman, T.E., Nagler, P.L., Hernandez, M., and Goodrich, D.C., 2008, Multiyear riparian evapotranspiration and groundwater use for a semiarid watershed: Journal of Arid Environments, v. 72, no. 7, p. 1232–1246. https://doi.org/10.1016/j.jaridenv.2008.01.001.

Scott, R.L., Huxman, T.E., Barron-Gafford, G.A., Jenerette, G.D., Young, J.M., and Hamerlynck, E.P., 2014, When vegetation change alters ecosystem water availability: Global Change Biology, v. 20, no. 7, p. 2198–2210.

Scott, R.L., Shuttleworth, W.J., Goodrich, D.C., and Maddock, T., III, 2000, The water use of two dominant vegetation communities in a semiarid riparian ecosystem: Agricultural and Forest Meteorology, v. 105, nos. 1–3, p. 241–256.

Smith, D.W., Moreo, M.T., Buto, S.G., and Nelson, N.C., 2020, Supplemental evapotranspiration gap-filled datasets from Stump Spring and Hiko Springs, Clark County, southern Nevada, 2016–18: U.S. Geological Survey data release, https://doi.org/10.5066/P9KD11GX.

Smith, D.W., Moreo, M.T., Garcia, C.A., Halford, K.J., and Fenelon, J.M., 2017, A process to estimate net infiltration using a site-scale water-budget approach, Rainier Mesa, Nevada National Security Site, Nevada, 2002–05: U.S. Geological Survey Scientific Investigations Report 2017–5078, 22 p., https://doi.org/10.3133/sir20175078.

Smith, J.L., Laczniak, R.J., Moreo, M.T., and Welborn, T.L., 2007, Mapping evapotranspiration units in the Basin and Range carbonate-rock aquifer system, White Pine County, Nevada, and adjacent parts of Nevada and Utah: U.S. Geological Survey Scientific Investigations Report 2007–5087, 20 p., https://pubs.usgs.gov/sir/2007/5087/.

Stannard, D.I., Blanford, J.H., Kustas, W.P., Nichols, W.D., Amer, S.A., Schmugge, T.J., and Weltz, M.A., 1994, Interpretation of surface flux measurements in heterogeneous terrain during the Monsoon ’90 experiment: Water Resources Research, v. 30, no. 5, p. 1227–1239.

Stannard, D.I., Gannett, M.W., Polette, D.J., Cameron, J.M., Waibel, M.S., and Spears, J.M., 2013, Evapotranspiration from wetland and open-water sites at Upper Klamath Lake, Oregon, 2008–2010: U.S. Geological Survey Scientific Investigations Report 2013–5014, 66 p., https://pubs.usgs.gov/sir/2013/5014/.

Steinberg, P., 2001, *Prosopis glandulosa*, *in* Fire effects information system: Database of U.S. Department of Agriculture, Forest Service, Rocky Mountain Research Station, Fire Sciences Laboratory (Producer), accessed June 12, 2015, at https://www.fs.fed.us/database/feis/.

Stonestrom, D.A., Prudic, D.E., Laczniak, R.J., Akstin, K.C., Boyd, R.A., and Henkelman, K.K., 2003, Estimates of deep percolation beneath native vegetation, irrigated fields, and the Amargosa-River channel, Amargosa Desert, Nye County, Nevada: U.S. Geological Survey Open-File Report 2003–104, 88 p.

Stonestrom, D.A., Prudic, D.E., Walvoord, M.A., Abraham, J.D., Stewart-Deaker, A.E., Glancy, P.A., Constantz, J., Laczniak, R.J., and Andraski, B.J., 2007, Focused ground-water recharge in the Amargosa Desert Basin, *in* Stonestrom, D.A., Constantz, J., Ferre, T.P.A., and Leake, S.A., eds., Ground-water recharge in the arid and semiarid southwestern United States: U.S. Geological Survey Professional Paper 1703–E, p. 107–136., https://pubs.usgs.gov/pp/pp1703/e.

Swinbank, W.C., 1951, The measurement of vertical transfer of heat and water vapor by eddies in the lower atmosphere: Journal of Meteorology, v. 8, no. 3, p. 135–145.

Tanner, B.D., and Greene, J.P., 1989, Measurement of sensible heat and water-vapor fluxes using eddy-correlation methods—Final report prepared for U.S. Army Dugway Proving Grounds—Dugway, Utah, U.S. Army, 17 p.

Taylor, J.R., 1997, Error analysis—The study of uncertainties in physical measurements: Sausalito, California, University Science Books, 327 p.

Toth, J., 1963, A theoretical analysis of groundwater flow in small drainage basins: Journal of Geophysical Research, v. 68, no. 16, p. 4795–4812.

Twine, T.E., Kustas, W.P., Norman, J.M., Cook, D.R., Houser, P.R., Meyers, T.P., Prueger, J.H., Starks, P.J., and Wesely, M.L., 2000, Correcting eddy-covariance flux underestimates over a grassland: Agricultural and Forest Meteorology, v. 103, p. 279–300.

U.S. Department of Agriculture, 2012, National Agriculture Imagery Program (NAIP) information sheet: U.S. Department of Agriculture information sheet, accessed April 15, 2019, at https://www.fsa.usda.gov/Internet/FSA_File/naip_2012_final.pdf.

U.S. Department of Interior, 2001, The Federal Land Policy and Management Act of 1976, as amended: U.S. Department of Interior, Bureau of Land Management Office of Public Affairs, Washington D.C., 69 p., https://www.blm.gov/or/regulations/files/FLPMA.pdf.

U.S. Geological Survey, 2019, National Water Information System: U.S. Geological Survey web page, accessed June 20, 2019, at https://dx.doi.org/10.5066/F7P55KJN.

Webb, E.K., Pearman, G.I., and Leuning, R., 1980, Correction of flux measurements for density effects due to heat and water vapour transfer: Quarterly Journal of the Royal Meteorological Society, v. 106, p. 85–100.

White, W.N., 1932, A method of estimating ground-water supplies based on discharge by plants and evaporation from soil—Results of investigations in Escalante Valley, Utah, *in* Contributions to the hydrology of the United States 1932: U.S. Geological Survey Water-Supply Paper 659–A, 105 p., 1 pl., https://pubs.er.usgs.gov/publication/wsp659A.

Wilson, K., Goldstein, A., Falge, E., Aubinet, M., Baldocchi, D., Berbigier, P., Bernhofer, C., Ceulemans, R., Dolman, H., Field, C., Grelle, A., Ibrom, A., Law, B., Kowalski, A., Meyers, T., Moncrieff, J., Monson, R., Oechel, W., Tenhunen, J., Valentini, R., and Verma, S., 2002, Energy balance closure at FLUXNET sites: Agricultural and Forest Meteorology, v. 113, p. 223–243.

Winograd, I.J., and Thordarson, W., 1975, Hydrogeologic and hydrochemical framework, south-central Great Basin, Nevada-California, with special reference to the Nevada test site: U.S. Geological Survey Professional Paper 712–C, 126 p., https://pubs.er.usgs.gov/publication/pp712C.

Yang, D., Goodison, B.E., Metcalfe, J.R., Golubev, V.S., Bates, R., Pangburn, T., and Hanson, C.L., 1998, Accuracy of NWS 8″ standard nonrecording precipitation gauge—Results and application of WMO intercomparison: Journal of Atmospheric and Oceanic Technology, v. 15, p. 54–68.

Zaimes, G., Nichols, M., and Green, D., 2007, Characterization of riparian areas, *in* Zaimes, G., ed., Understanding Arizona's riparian areas: University of Arizona cooperative extension publication AZ1432, https://extension.arizona.edu/sites/extension.arizona.edu/files/pubs/az1432.pdf.

Appendix 1. Selected Daily Evapotranspiration, Energy Balance, and Meteorological Data, Stump Spring and Hiko Springs, 2016–18

The data distributed as part of this report are in Microsoft® Excel® for Office 365 format. Column headers are described within the spreadsheet. Selected daily data and plots are presented. Eddy covariance latent- and sensible-heat flux data, and actual evapotranspiration data, are not corrected for energy imbalances at daily time steps. Appendix 1 is available for download at https://doi.org/10.3133/sir20205075. Sub-daily (30-minute) datasets also are available for download at https://nevada.usgs.gov/et/.

Publishing support provided by the U.S. Geological Survey
Science Publishing Network, Tacoma Publishing Service Center

For more information concerning the research in this report, contact the
Director, Nevada Water Science Center
U.S. Geological Survey
2730 N. Deer Run Road
Carson City, Nevada 89701
https://www.usgs.gov/centers/nv-water

ISSN 2328-0328 (online)
https://doi.org/10.3133/sir20205075